



Modeling stress–strain state of cancellous bone tissue fragments in compression

Tatyana V. Chaykovskaya, Ekaterina S. Marchenko, Yuri F. Yasenchuk, Gulsharat A. Baigonakova & Alex A. Volinsky

To cite this article: Tatyana V. Chaykovskaya, Ekaterina S. Marchenko, Yuri F. Yasenchuk, Gulsharat A. Baigonakova & Alex A. Volinsky (07 Jan 2025): Modeling stress–strain state of cancellous bone tissue fragments in compression, *Mechanics of Advanced Materials and Structures*, DOI: [10.1080/15376494.2024.2448609](https://doi.org/10.1080/15376494.2024.2448609)

To link to this article: <https://doi.org/10.1080/15376494.2024.2448609>



Published online: 07 Jan 2025.



Submit your article to this journal [↗](#)




View related articles [↗](#)



View Crossmark data [↗](#)

Modeling stress–strain state of cancellous bone tissue fragments in compression

Tatyana V. Chaykovskaya^a , Ekaterina S. Marchenko^a, Yuri F. Yasenchuk^a, Gulsharat A. Baigonakova^a, and Alex A. Volinsky^{a,b}

^aLaboratory of Medical Alloys and Implants with Shape Memory, National Research Tomsk State University, Tomsk, Russia;

^bDepartment of Mechanical Engineering, University of South Florida, Tampa, FL, USA

ABSTRACT

The article examines the stress–strain state of model cancellous bone tissue fragments under compression, replicating the architecture of natural bone. The study focuses on the impact of principal trabeculae length and mineral content on the stress–strain state and effective elastic modulus. Findings show that deformation response varies with trabeculae structure and mineral mass, with significant normal strains and von Mises stress localized in the surface layers of shorter trabeculae. The effective elastic modulus decreases with trabeculae length. The results underscore the need to explore additional parameters for designing mechanically compatible osteoimplants. Model results align with natural bone behavior.

ARTICLE HISTORY

Received 9 September 2024

Accepted 27 December 2024

KEYWORDS

Cancellous bone tissue; uniaxial compression; mechanics; elastic modulus; model fragment

1. Introduction

New methods for treating oncological diseases and restoring impaired parts of the body using porous implants to replace bone defects are being actively developed. These methods promote social rehabilitation, provide patients with improved quality of life, and ultimately extend life expectancy. The development and selection of biochemically compatible materials for bone grafts are necessary but not sufficient conditions for implant survival in the body. Mechanical compatibility is also crucial for the integrity of the bone graft and natural bone. The bone structure, composition, and corresponding mechanical properties adapt to changing external mechanical conditions (Wolff's law [1]), vary within the same bone, and are different in different individuals [2–10]. Therefore, the same implant may survive in one patient and not survive in another. Thus, it is necessary to study changes in the mechanical behavior of a certain type of bone tissue (cancellous and/or compact) when changing their structure and composition in order to develop and select a definite implant type.

Multiple studies investigated the mechanical behavior of bones and bone tissues using computer modeling and experimental methods [11–25]. Computer modeling methods used to study the mechanical behavior of bone tissues show a number of advantages over experiments. These methods eliminate the need to extract the examined part of the bone, taking into account various structural features of the bone tissue and allowing assessment of the stresses and

strains distribution in the bone tissue under a certain type of loading.

Most of the studies addressing computer modeling include 3D geometric models of cancellous bone tissue fragments developed based on the computed tomography images [15, 16, 22–25] and include geometric features of the structure and bone mechanics in a particular patient, which do not allow generalized conclusions about the mechanical behavior of bone tissue, in contrast to the models with parametric variation of characteristics.

Existing modern studies typically determine the modulus of elasticity and the ultimate strength for the selection and development of osteoimplants. Nevertheless, the question of the implant's osseointegration remains open, as the number of implant replacement surgeries due to its loosening as a result of peri-implant bone resorption remains at the same level [26–30]. As noted above, bone tissue is a smart material because it adapts to changing mechanical conditions, so studying its mechanical response requires nontraditional approaches that are different from artificial materials.

The magnitude and nature of stress and strain distribution in bone tissues determine the areas of placement of bone cells, osteoclasts, and osteoblasts after implantation [31–33]. It is likely that changes in the magnitude and nature of stress and strain distribution in bone tissues associated with implant insertion serve as mechanical stimuli for restructuring bone tissue at the bone–implant interface. Therefore, the selection of osteoimplants should be carried out according to effective mechanical parameters

that determine the nature and magnitude of the realized stresses and deformations of the bone fragment being replaced.

The following tasks were set in this study:

- Determine mechanical characteristics that reflect the magnitude and nature of stress and strain distribution in cancellous bone tissue for the development and selection of individual mechanically compatible osteoimplants based on computer modeling of the stress–strain state of spongy bone tissue fragments with different structure and composition.
- Investigate how the nature and magnitude of stress and strain distribution change with the structure and composition of cancellous bone tissue to obtain general features of their changes under uniaxial compression.

This study considers the mechanical behavior of geometrically idealized model fragments of cancellous bone tissue. Model fragments of cancellous bone tissue are explicitly constructed using a trabecular model [34, 35] with trabeculae represented as rods of variable thickness arranged in trabecular nodes. A set of trabecular nodes forms a model bone tissue fragment. The algorithm for constructing geometric models of cancellous bone tissue enables rebuilding the structure of a model fragment by varying the structural parameters (length and thickness) of trabeculae. The model implicitly takes into account collagen and mineral components of the bone by setting the effective elastic modulus of trabeculae.

2. Materials and methods

2.1. Trabecular model of cancellous bone tissue

A trabecular node is taken as a structural element of model fragments of cancellous bone tissue in Figure 1. A trabecular node includes a central sphere with six half-

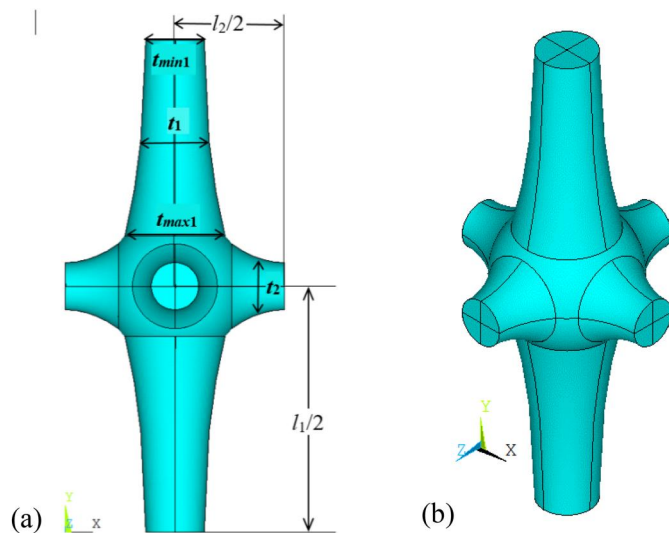


Figure 1. Trabecular node as a structural element of model bone fragments: (a) front view; (b) 3D view.

length trabeculae H1 and H2. Of these, two trabeculae are located along the Y axis that coincides with the loading direction, and four trabeculae are located in two mutually perpendicular directions along the X and Z axes. The thickness of each trabecula in the area of its contact with the central sphere t_{\max} and in the region of half the length t_{\min} in Figure 1 is calculated from a given average value of the trabecular thickness t using the expression in Ref. [36] obtained from experimental data. A model fragment of cancellous bone tissue is a set of trabecular nodes.

The algorithm for constructing model fragments of cancellous bone tissue enables computer-aided rebuilding of geometric models with regard to the length and average thickness of trabeculae. Trabeculae oriented along the loading axis are considered principal, and trabeculae located perpendicular to the loading axis are considered secondary. All parameters related to the principal trabeculae have an index 1, and those related to the secondary ones have an index 2. The length of the principal trabeculae l_1 was varied from 0.215 to 1.3 mm, the length of the secondary trabeculae was set constant $l_2=0.215$ mm, and the average secondary trabeculae thickness t_2 was varied from 0.109 to 0.162 mm [18], while the thickness of the principal trabeculae was set constant $t_1=0.162$ mm.

Representative volume elements of the model cancellous bone tissue fragments of different architecture were constructed, corresponding to the architecture of natural cancellous tissue fragments taken from the epiphysis of the femur of a bull in Figure 2, highlighted with black rectangles. Fragments of natural spongy tissue of the femur of a bull were purchased from farmers. The Y axis corresponds to the longitudinal axis of the bone sample, in which direction the main trabeculae are predominantly aligned. Representative volume elements contain 27 trabecular nodes. The model volume element with the length of the principal trabecula exceeding the length of the secondary one contains elongated pores in Figure 2(a) and (b). The volume element with equal trabecula lengths contains round pores in Figure 2(c).

2.2. Material definition

The material of the bone trabeculae was considered homogeneous and isotropic. Bone trabeculae were regarded as a two-phase composite material. The effective elastic modulus of trabeculae was calculated using the expression of the mechanics of composite materials taken for the case of hydroxyapatite fibers arbitrarily oriented in the collagen matrix [37]. The elastic modulus of collagen and hydroxyapatite was taken as 10 MPa and 35 GPa, respectively. The mass fraction of hydroxyapatite minerals α was varied from 0.1 to 0.4. Therefore, the calculated elastic modulus ranged from 295 to 1436 MPa, which is in line with the data reported in Ref. [38]. Poisson's ratio of trabeculae was taken as 0.3.

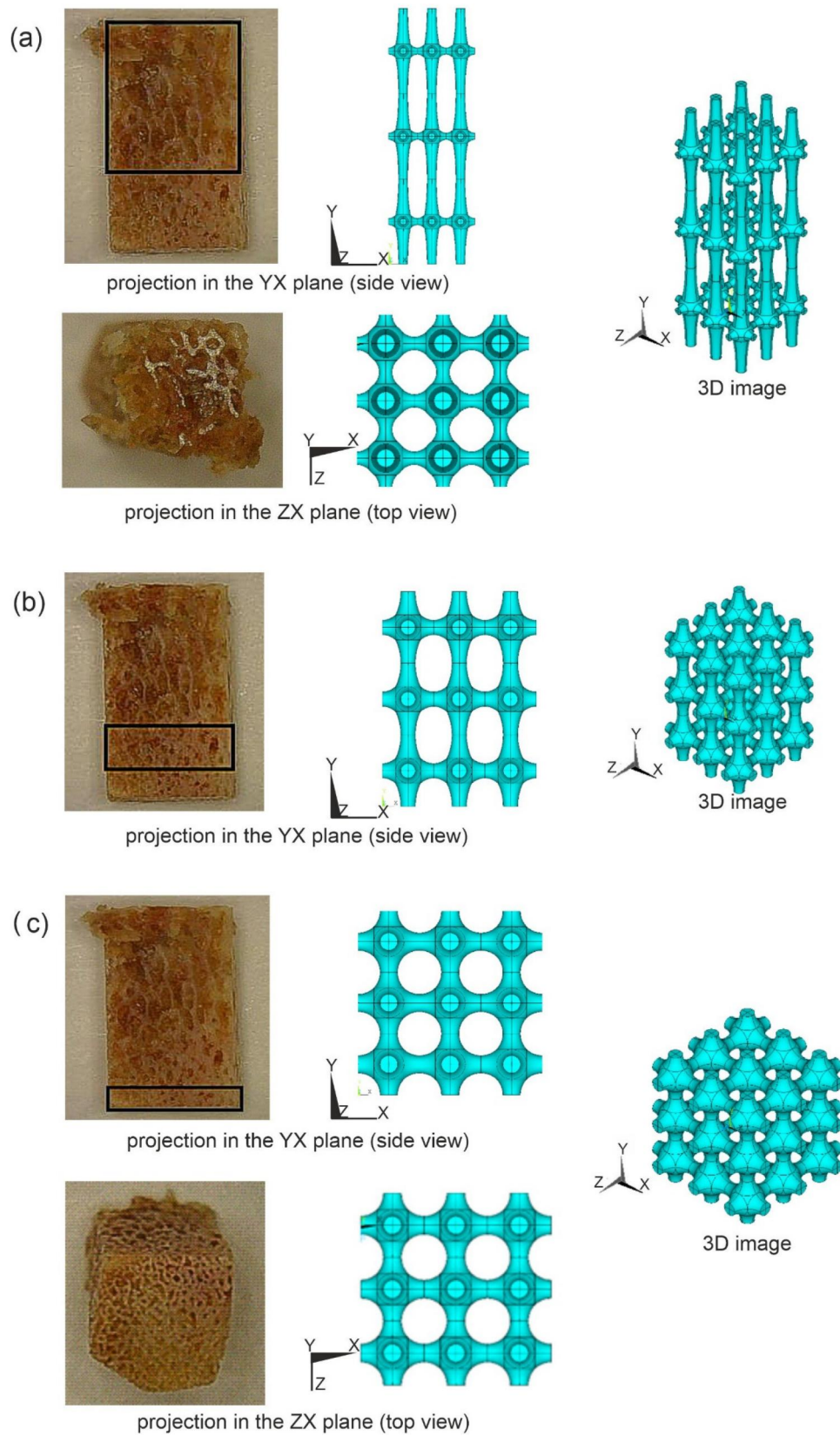


Figure 2. Architecture of natural cancellous bone tissue fragments and the corresponding model fragments: (a) $l_1 = 1.31$ mm, $l_2 = 0.215$ mm; (b) $l_1 = 0.383$ mm, $l_2 = 0.215$ mm; (c) $l_1 = 0.215$ mm, $l_2 = 0.215$ mm.

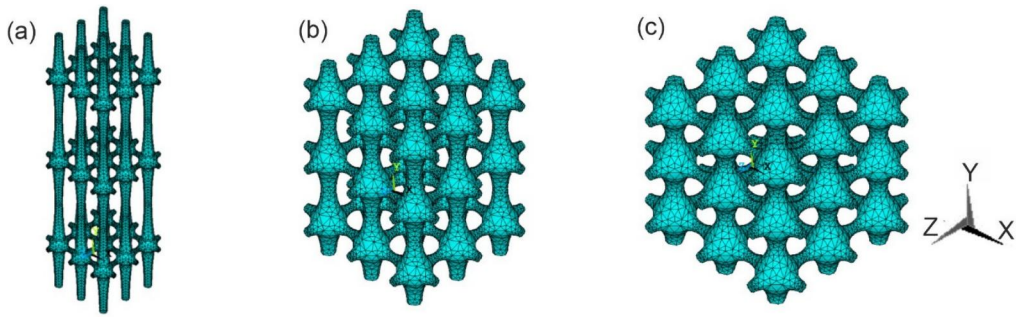


Figure 3. Examples of finite element models of cancellous bone tissue fragments ($l_2 = 0.215$ mm, $t_1 = 0.162$ mm, $t_2 = 0.109$ mm) with different lengths of the principal trabeculae: (a) $l_1 = 1.31$ mm (56,249 finite elements), (b) $l_1 = 0.383$ mm (40,224 finite elements), (c) $l_1 = 0.215$ mm (39,403 finite elements).

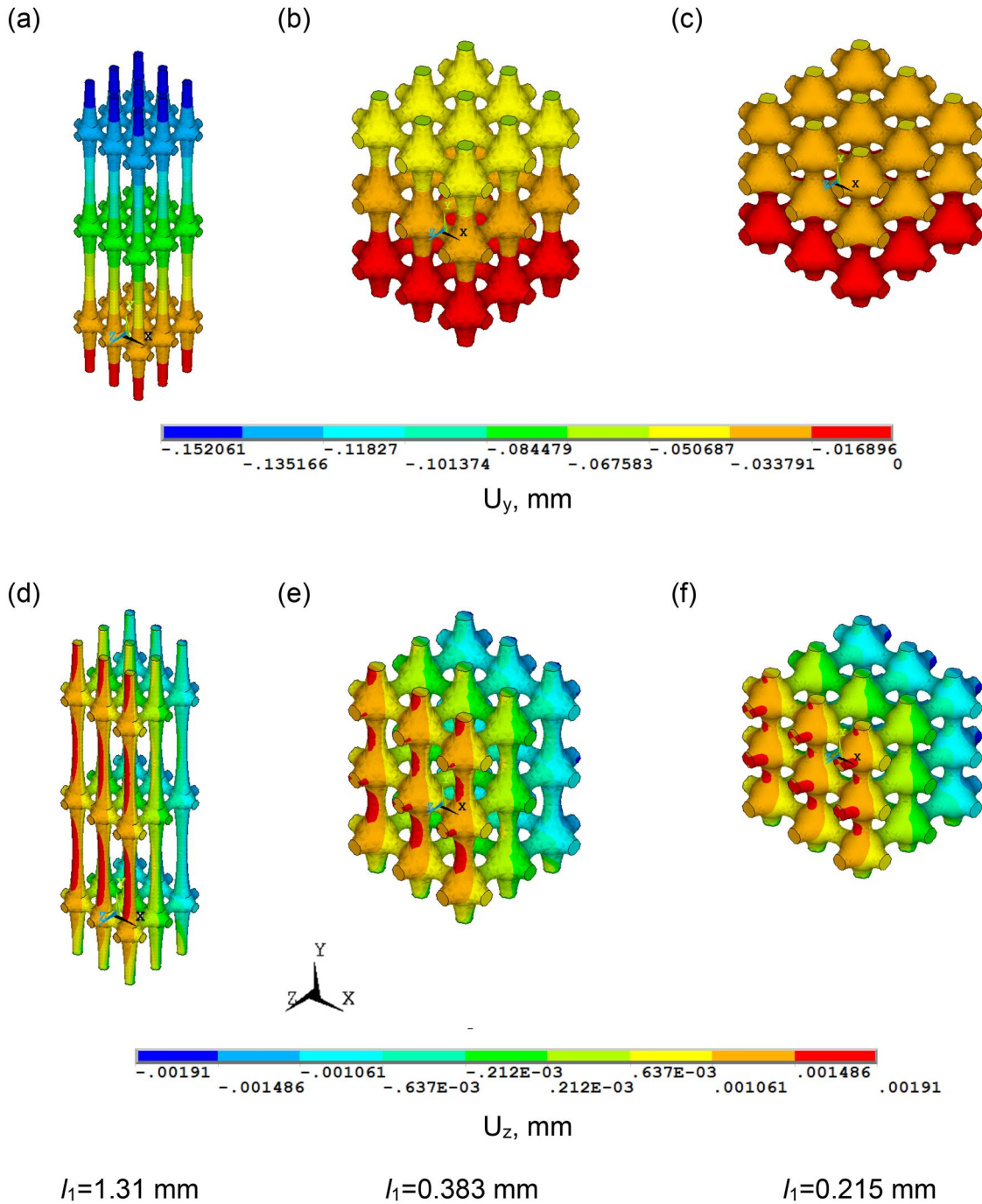


Figure 4. Distribution of displacements U_y and U_z in model cancellous bone tissue samples with different lengths of the principal trabecula: (a, d) $l_1 = 1.31$ mm, (b, e) $l_1 = 0.383$ mm, (c, f) $l_1 = 0.215$ mm. Here, $l_2 = 0.215$ mm, $t_1 = 0.162$ mm, $t_2 = 0.162$ mm, $\alpha = 0.1$.

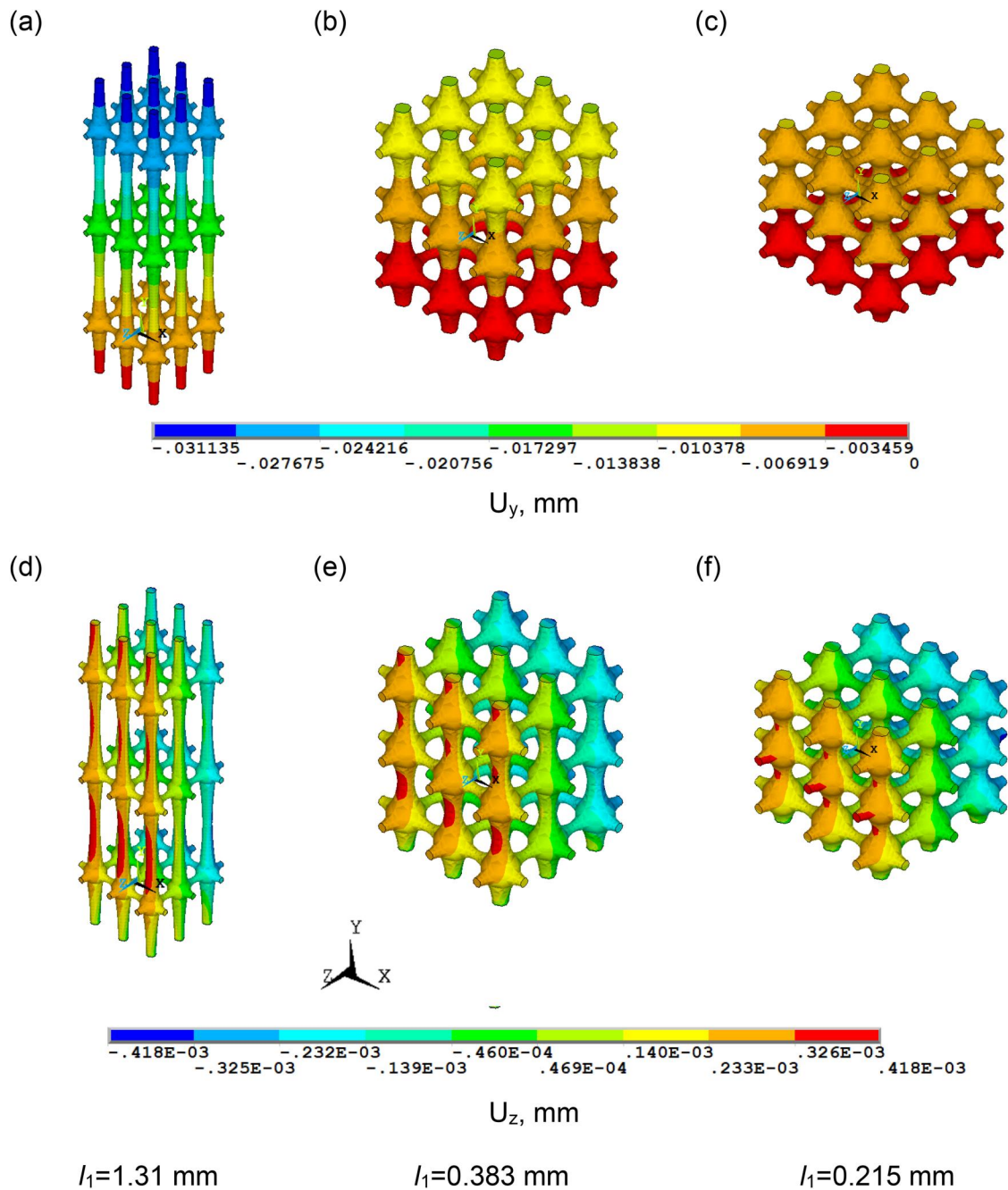


Figure 5. Distribution of displacements U_y and U_z in model cancellous bone tissue samples with different lengths of the principal trabecula: (a, d) $l_1 = 1.31 \text{ mm}$, (b, e) $l_1 = 0.383 \text{ mm}$, (c, f) $l_1 = 0.215 \text{ mm}$. Here, $l_2 = 0.215 \text{ mm}$, $t_1 = 0.162 \text{ mm}$, $t_2 = 0.109 \text{ mm}$, $\alpha = 0.4$.

2.3. Finite element mesh

The stress-strain state of model cancellous bone tissue fragments was calculated by the linear theory of elasticity using the finite element method in the ANSYS software package. Figure 3 illustrates examples of the finite element models. An irregular finite element mesh with tetrahedral 3-D 20-node finite elements was used to build the finite element models. The number of finite elements used to calculate the stress-strain state was determined based on the grid

convergence of the calculation results. The average volume of the final element is 10^{-5} mm^3 . The error percentage in mesh sensitivity analysis is $<2\%$.

2.4. Boundary conditions

Model fragments of cancellous bone tissue were exposed to static uniaxial compression along the Y axis. The lower ZX plane of the samples was rigidly fixed, and

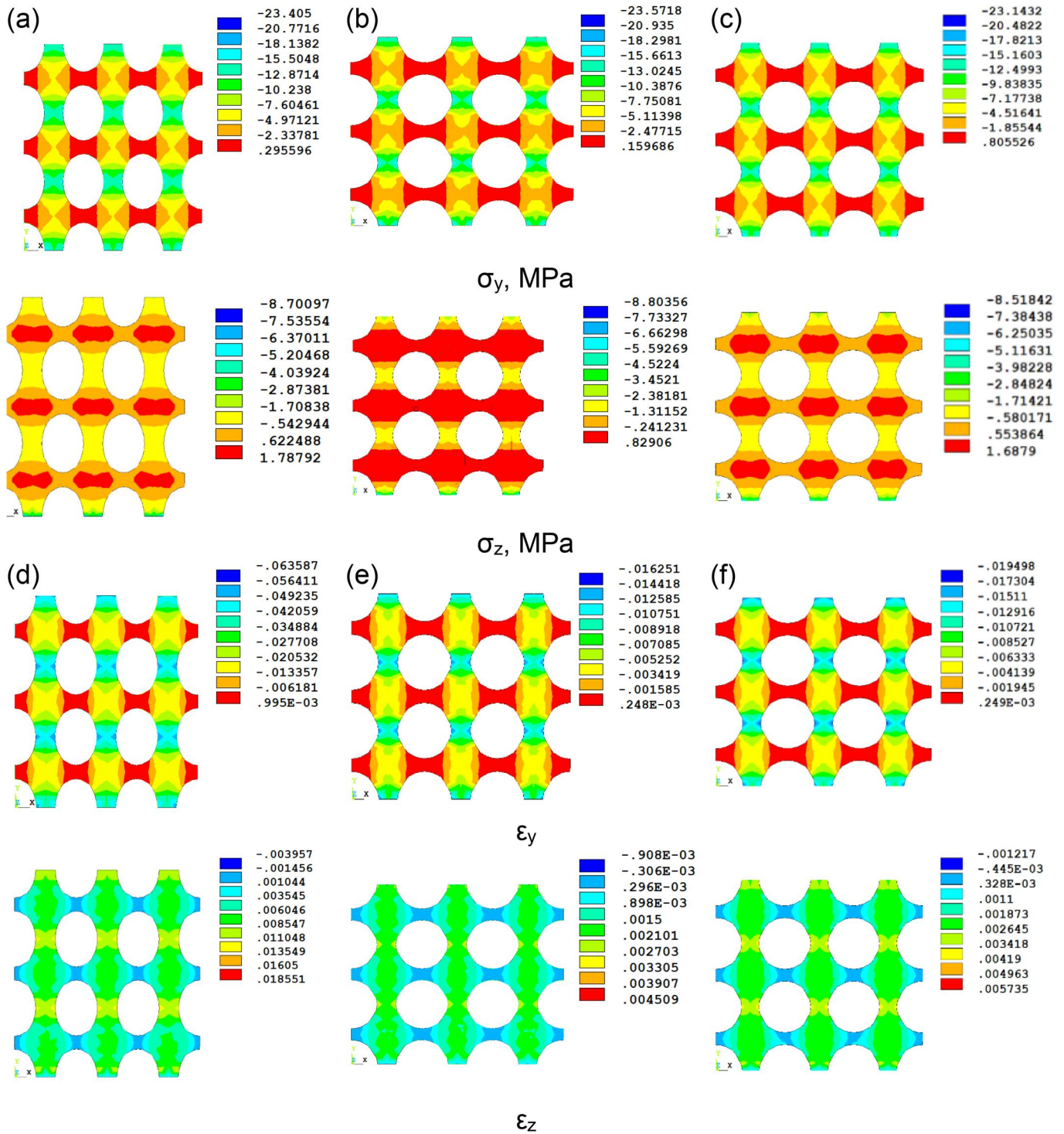


Figure 6. Distribution of (a, b, c) normal stresses and (d, e, f) strains in sections of model samples of cancellous bone tissue with different structure and composition: (a, d) $t_1 = 0.215$ mm, $t_2 = 0.162$ mm, $l_1 = 0.383$ mm, $l_2 = 0.215$ mm, $\alpha = 0.1$; (b, e) $t_1 = 0.162$ mm, $t_2 = 0.109$ mm, $l_1 = 0.215$ mm, $l_2 = 0.215$ mm, $\alpha = 0.34$; (c, f) $t_1 = 0.150$ mm, $t_2 = 0.109$ mm, $l_1 = 0.215$ mm, $l_2 = 0.215$ mm, $\alpha = 0.3$.

Table 1. The effective mechanical parameters of cancellous bone tissue with different structures and compositions.

Fragment number	Structure and composition parameters	Effective longitudinal elastic modulus E (GPa)	mU_i		
			mU_x	mU_y	mU_z
1 Figure 6(a, d)	$t_1 = 0.215$ mm, $t_2 = 0.162$ mm, $l_1 = 0.383$ mm, $l_2 = 0.215$ mm, $\alpha = 0.1$	0.5	0.04	0.92	0.04
2 Figure 6(b, e)	$t_1 = 0.162$ mm, $t_2 = 0.109$ mm, $l_1 = 0.215$ mm, $l_2 = 0.215$ mm, $\alpha = 0.34$	2.2	0.05	0.90	0.05
3 Figure 6(c, f)	$t_1 = 0.150$ mm, $t_2 = 0.109$ mm, $l_1 = 0.215$ mm, $l_2 = 0.215$ mm, $\alpha = 0.3$	1.9	0.04	0.92	0.04
4	$t_1 = 0.162$ mm, $t_2 = 0.135$ mm, $l_1 = 0.383$ mm, $l_2 = 0.215$ mm, $\alpha = 0.36$	2.2	0.03	0.94	0.03

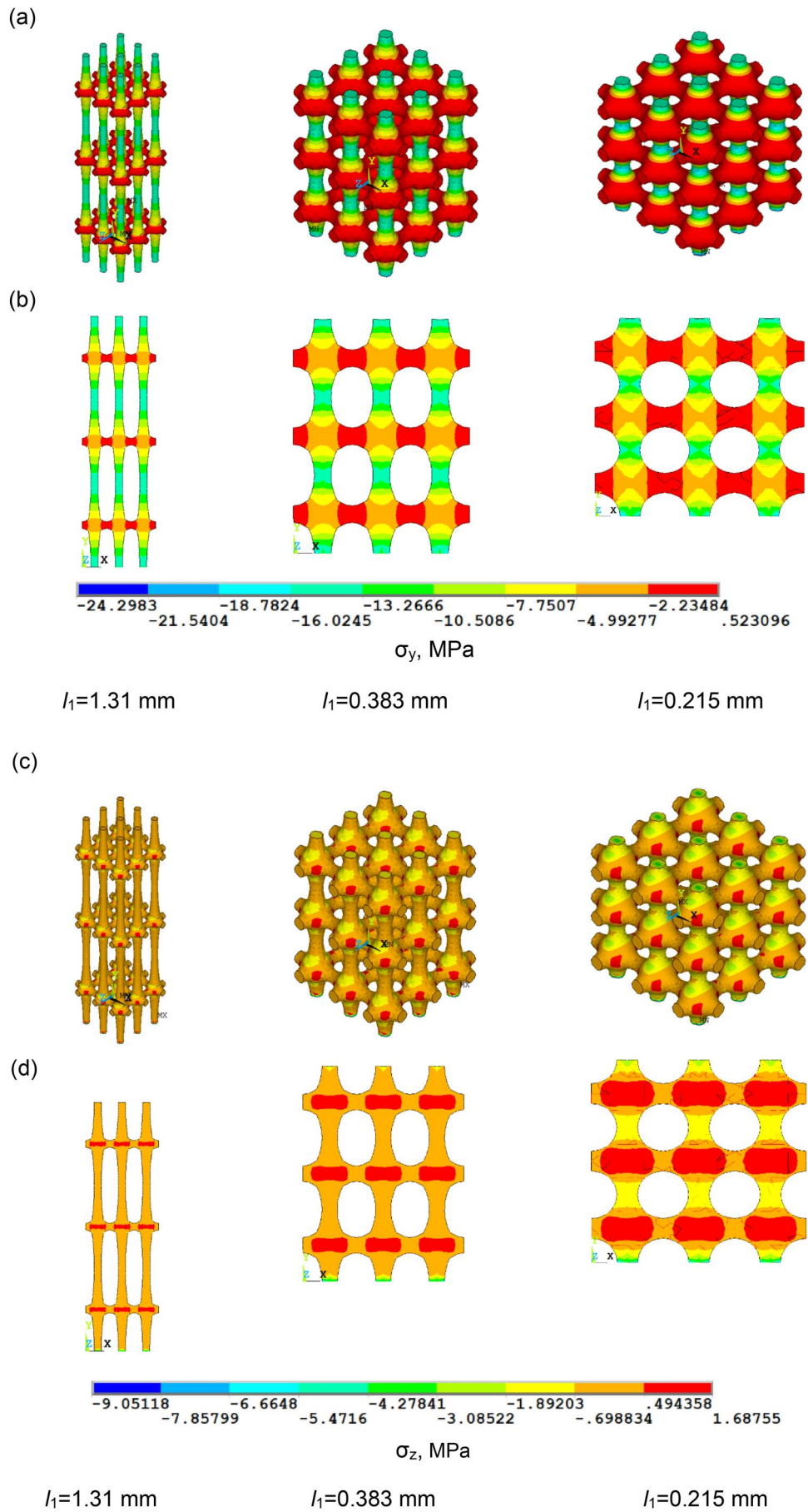


Figure 7. Distribution of normal stresses (a, c) over the surface and (b, d) inside model samples of cancellous bone tissue (section formed by the YX plane) with different lengths of the principal trabecula. Here, $l_2 = 0.215$ mm, $t_1 = 0.162$ mm, $t_2 = 0.162$ mm, $\alpha = 0.1$.

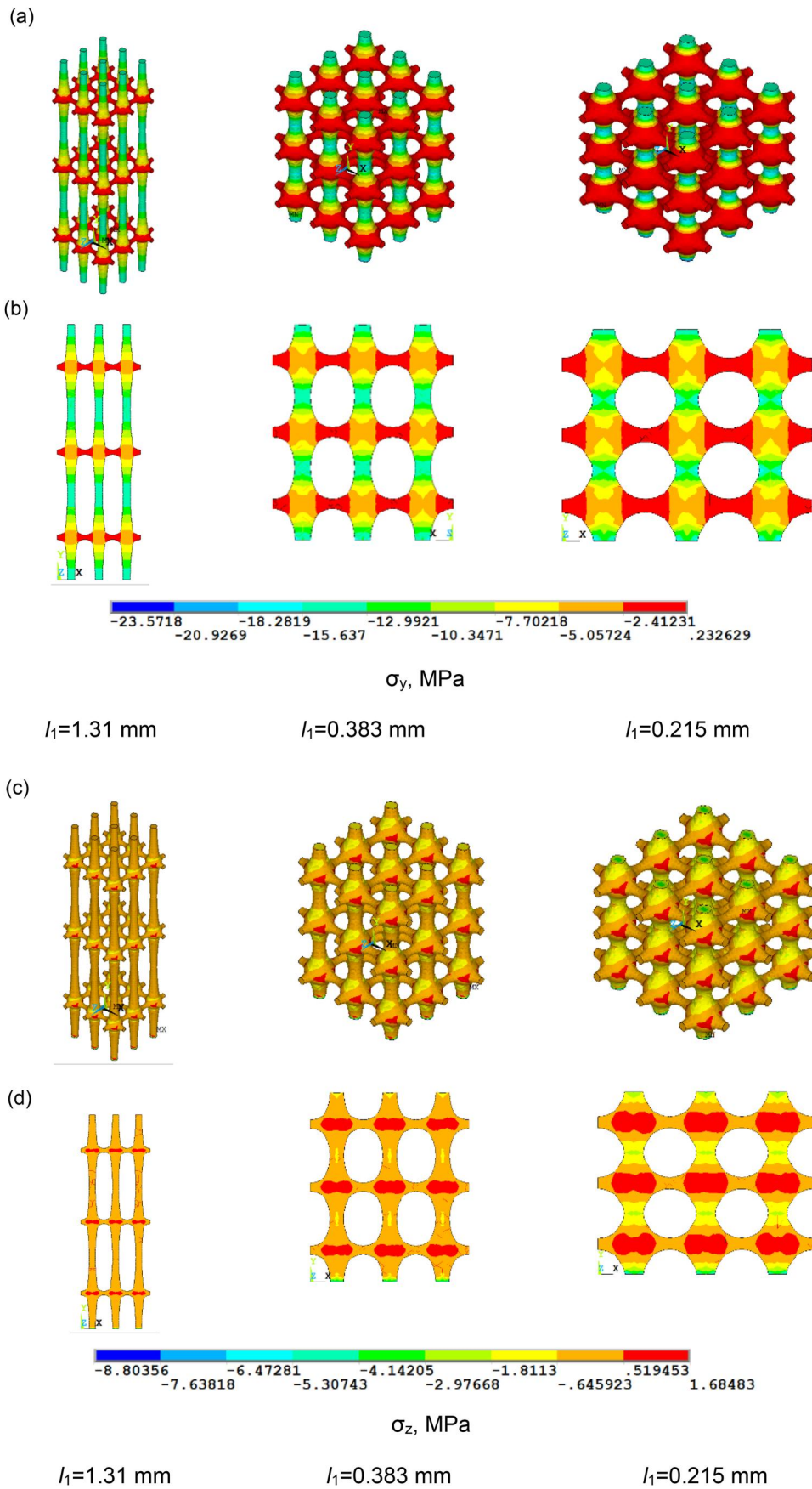


Figure 8. Distribution of normal stresses (a, c) over the surface and (b, d) inside model samples of cancellous bone tissue (section formed by the YX plane) with different lengths of the principal trabecula. Here, $l_2 = 0.215$ mm, $t_1 = 0.162$ mm, $t_2 = 0.109$ mm, $\alpha = 0.4$.

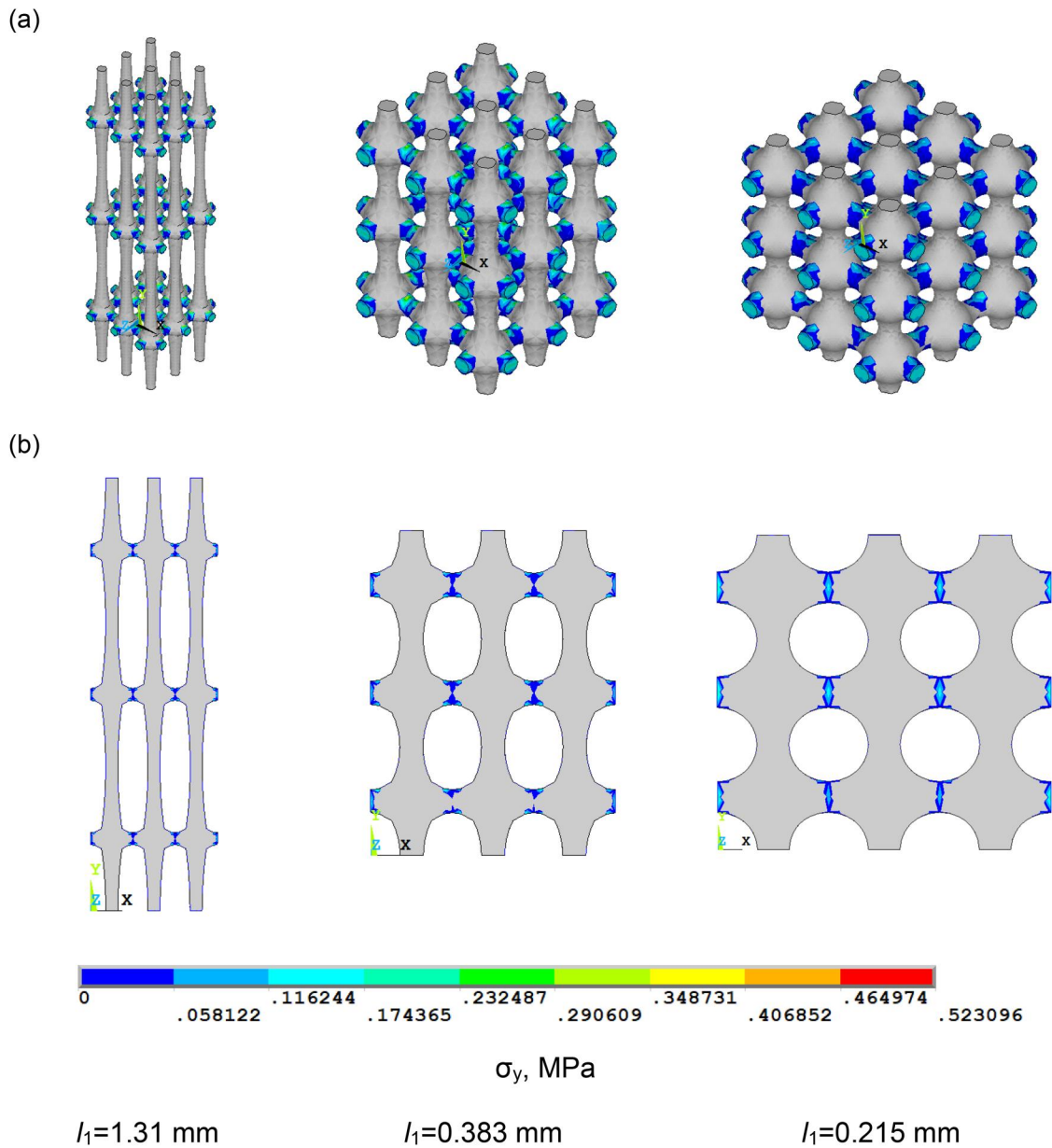


Figure 9. Distribution of tensile normal stresses (a, c) over the surface and (b, d) inside model samples of cancellous bone tissue (section formed by the YX plane) with different lengths of the principal trabecula. Here, $l_2 = 0.215 \text{ mm}$, $t_1 = 0.162 \text{ mm}$, $t_2 = 0.162 \text{ mm}$, $\alpha = 0.1$.

the upper plane was loaded with a compressive stress of 15 MPa. This value of compressive stress is below the ultimate strength of the bone tissue sample under consideration.

3. Results

3.1. Effective mechanical parameters of stresses and strains distribution in bone tissue model fragments

Studying deformation behavior of cancellous bone tissue model samples with different structures and mineral content under uniaxial compression revealed that three deformation types are realized to varying degrees in three mutually perpendicular directions in each sample. These

include compression in the direction of the applied load (along the Y axis) and tension in two mutually perpendicular directions (along the X and Z axes), as indicated by the displacement distributions in Figures 4 and 5. The distribution of displacements in the Z and X directions are identical; therefore, Figures 4 and 5 only show U_z displacements.

The regions of the maximum displacements belong to the principal trabeculae. The mU_x , mU_y , mU_z parameters have been introduced to assess the extent of manifestation of the aforementioned deformation responses of bone samples in three mutually perpendicular directions under uniaxial compression. These parameters are defined as the ratio of the maximum absolute displacement in one of the directions (X , Y , or Z) to the sum of the maximum

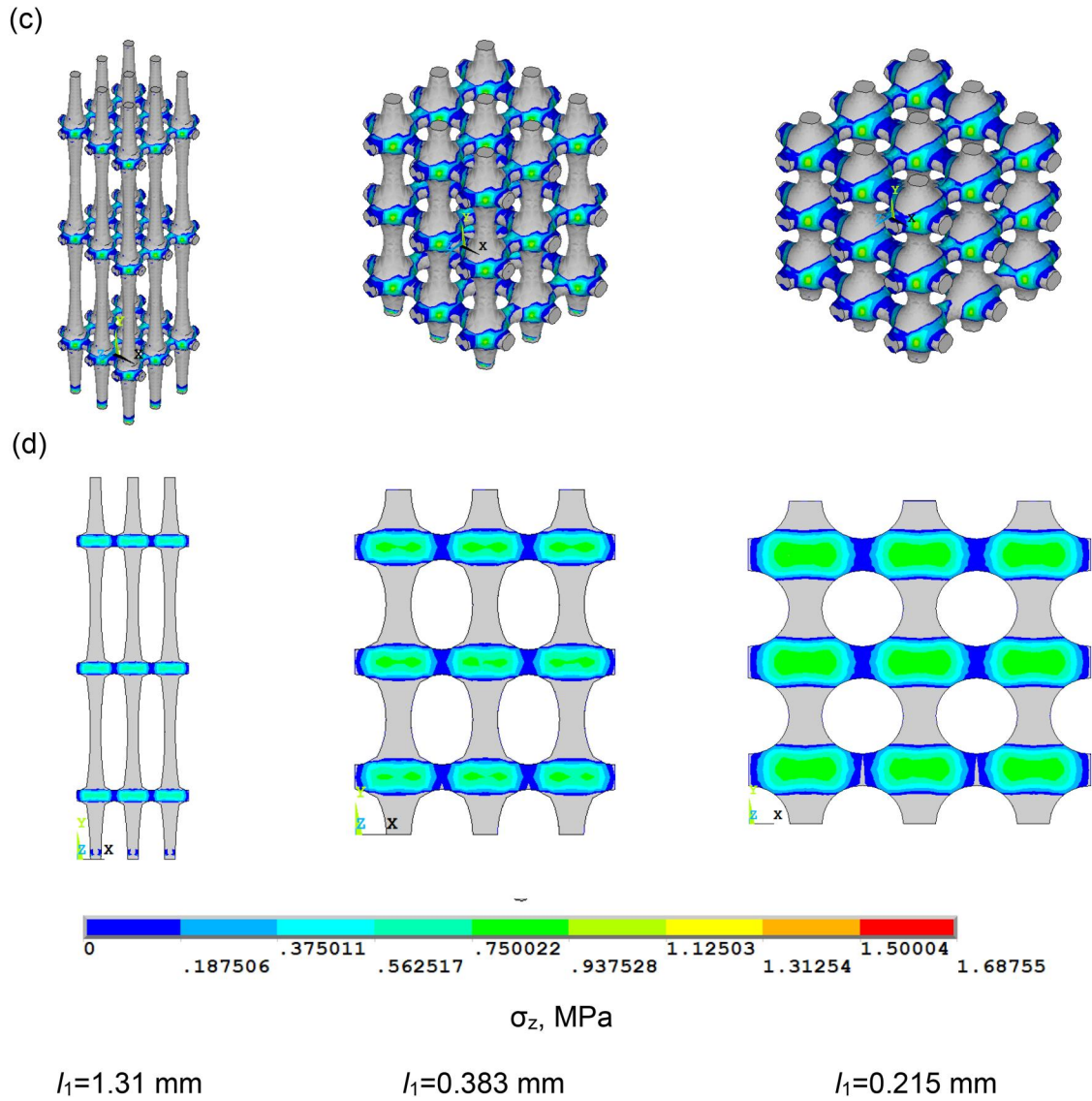


Figure 9. Continued.

absolute displacements in the three mutually perpendicular directions [39, 40].

$$\begin{aligned}
 mU_x &= \frac{\max|U_x|}{(\max|U_x| + \max|U_y| + \max|U_z|)}; \\
 mU_y &= \frac{\max|U_y|}{(\max|U_x| + \max|U_y| + \max|U_z|)}; \\
 mU_z &= \frac{\max|U_z|}{(\max|U_x| + \max|U_y| + \max|U_z|)}.
 \end{aligned} \quad (1)$$

Here, mU_y represents the extent of compression in the fragment of cancellous bone tissue, and mU_x , mU_z correspond to the tension along the X and Z axes, respectively. Figure 6 depicts the distributions of normal axial stresses and strains in the model fragments of cancellous bone tissue with different structures and compositions. The distributions of σ_z and σ_x stresses and ε_z and ε_x strains for each bone sample are symmetrical, and therefore, in Figure 6 and throughout the article, only σ_z and ε_z distributions are presented.

It can be seen from the presented figures that fragments of bone tissues with different structures and compositions may exhibit both similar and different patterns of stress and strain distribution. However, the magnitudes of stresses and strains vary. The similarity in the distribution patterns of stresses and strains is determined by the equal degree of the deformation response of bone tissue fragments in three mutually perpendicular directions under uniaxial compression. In other words, such samples have identical mU_x , mU_y , and mU_z parameters in Table 1.

The results presented in Figure 6 and Table 1 indicate that bone tissue fragments may have similar elastic moduli but differ in the nature of stress and strain distribution. Conversely, they may have a similar distribution of stresses and strains, i.e. identical parameters mU_x , mU_y , and mU_z , while having different elastic moduli in Table 1.

Thus, a fragment of cancellous bone tissue with $t_1=0.215$ mm, $t_2=0.162$ mm, $l_1=0.383$ mm, $l_2=0.215$ mm, $\alpha=0.1$ structure and composition parameters, and a fragment with $t_1=0.150$ mm, $t_2=0.109$ mm, $l_1=0.215$ mm,

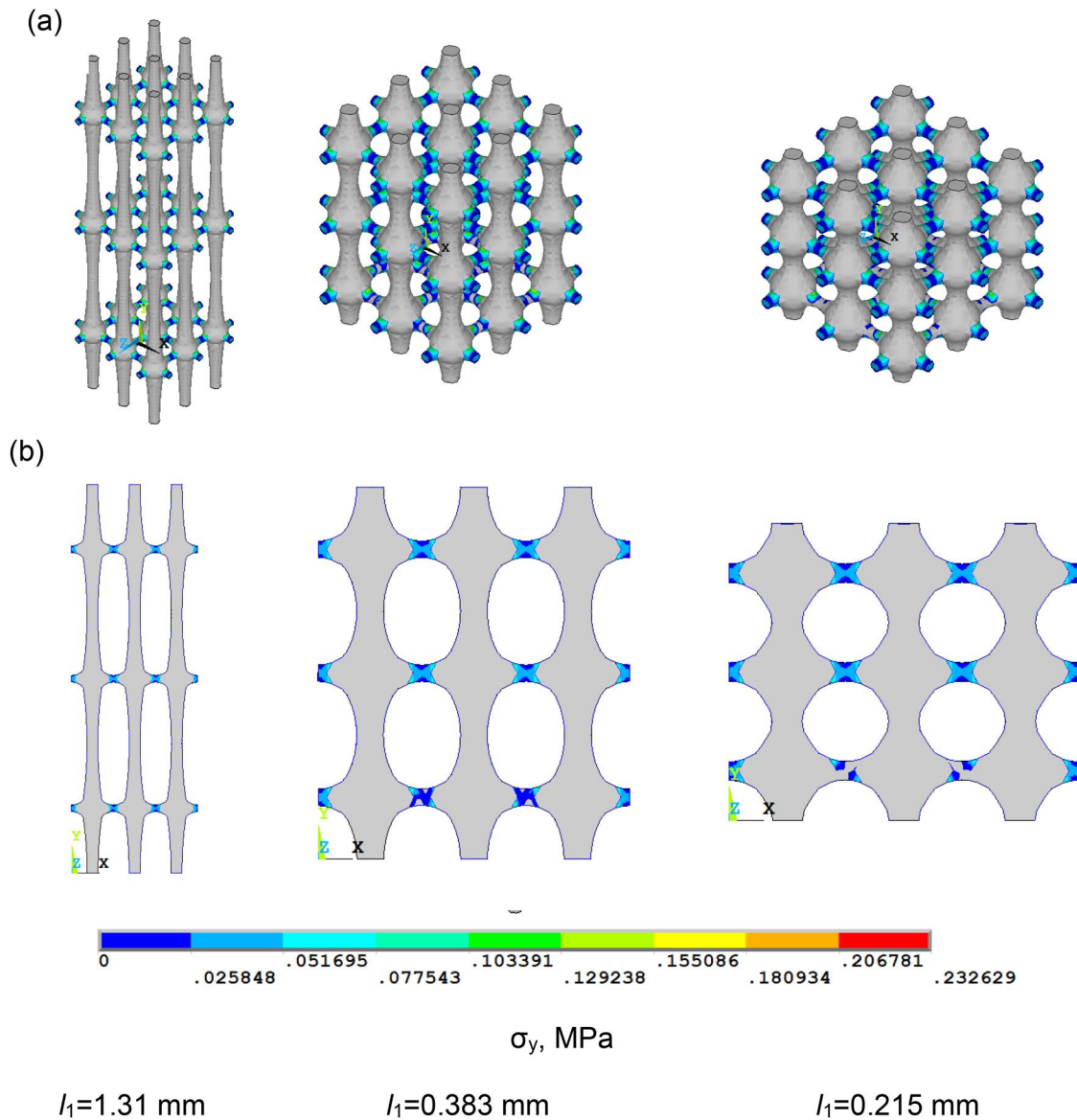


Figure 10. Distribution of tensile normal stresses (a, c) over the surface and (b, d) inside model samples of cancellous bone tissue (section formed by the YX plane) with different lengths of the principal trabecula. Here, $l_2 = 0.215$ mm, $t_1 = 0.162$ mm, $t_2 = 0.109$ mm, $\alpha = 0.4$.

$l_2=0.215$ mm, and $\alpha=0.3$ parameters exhibit identical stress and strain distribution patterns in Figure 6(a, d, c, f). In other words, they have the same parameters mU_x , mU_y , and mU_z but differ in elastic modulus (Table 1, fragments 1 and 3). Fragments of cancellous bone tissue 2 ($t_1=0.162$ mm, $t_2=0.109$ mm, $l_1=0.215$ mm, $l_2=0.215$ mm, $\alpha=0.34$), 3 ($t_1=0.150$ mm, $t_2=0.109$ mm, $l_1=0.215$ mm, $l_2=0.215$ mm, $\alpha=0.3$), and 4 ($t_1=0.162$ mm, $t_2=0.135$ mm, $l_1=0.383$ mm, $l_2=0.215$ mm, $\alpha=0.36$) have similar elastic moduli but differ in the nature of stress and strain distribution in Figure 6(b, e, c, f). They have different parameters mU_x , mU_y , and mU_z .

3.2. Principal trabeculae length and minerals mass fraction effects on the normal stresses distribution in cancellous bone tissue fragments

Figures 7 and 8 show distribution of normal stresses for the above samples over the surface and in the longitudinal

section formed by the YX plane. As seen from the figures, the highest absolute compressive stresses σ_y occur in the principal trabeculae, while the maximum tensile stresses occur in the secondary trabeculae in Figures 7–9 and 10(a, b). At increased length of the principal trabecula, the distribution pattern of axial stresses σ_y over the sample surface does not change in Figures 7(a) and 8(a). The changes in distribution of the stresses σ_y can be observed in Figures 7(b) and 8(b), namely, decreased absolute compressive stresses in the trabecular sphere and increased stresses in the principal trabeculae leading to a more uniform distribution. The maximum tensile stresses σ_x and σ_z occur on the sample surface at the contact points between the secondary trabeculae and the trabecular sphere in Figures 7(c), 8(c), 9(c), and 10(c) and inside the trabecular sphere in Figures 7(d), 8(d), 9(d), and 10(d). The maximum absolute compressive stresses σ_x and σ_z occur at the contact points between the principal trabecula

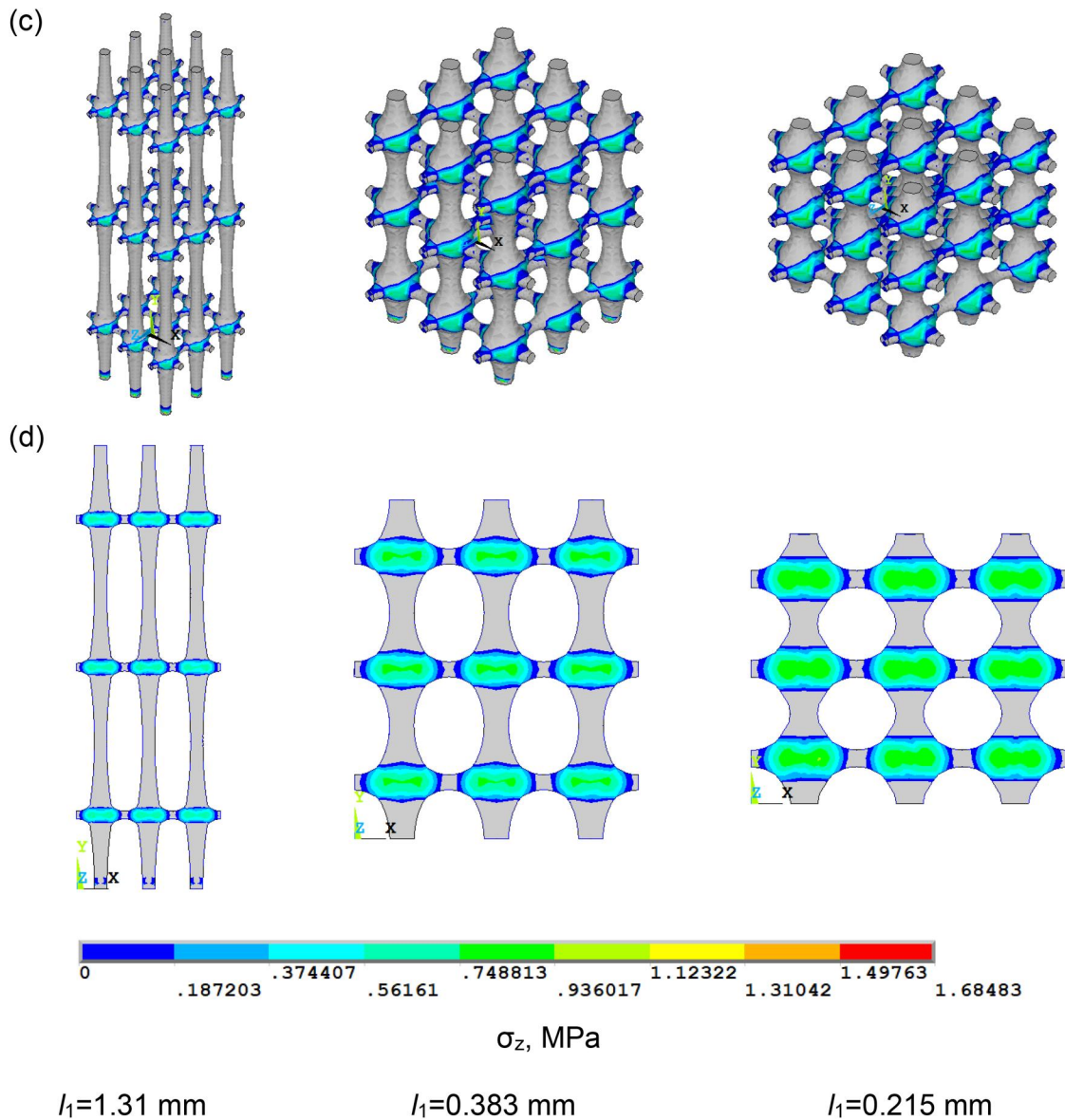


Figure 10. Continued.

and the trabecular sphere in Figures 7(c) and 8(c), and the stresses increase as the length of the principal trabecula is reduced. At increased length of the principal trabeculae, the compressive stresses σ_z and σ_x decrease in the region of the principal trabeculae in Figures 7(d) and 8(d). Comparison of the normal stresses σ_x , σ_y , and σ_z indicates that σ_z , σ_x are the maximum tensile normal stresses, and σ_y stresses are the maximum absolute compressive stresses.

A change in the thickness of the secondary trabeculae and a change in the mass fraction of minerals in the sample do not affect the values of the maximum and minimum normal stresses. A sixfold increase in the length of the principal trabecula from 0.215 to 1.31 mm leads to an increase in the maximum tensile normal stresses σ_x , σ_z and σ_y by a factor of 1.4, to a decrease in the absolute values of the maximum compression normal stresses σ_x and σ_z by a factor of 1.7 and σ_y by a factor of 1.16.

3.3. Influence of the principal trabeculae length and minerals mass fraction on the von Mises stress distribution

Figures 11 and 12 show distribution of equivalent von Mises stresses, which indicates that the maximum stresses for a sample with short principal trabeculae ($l_1=0.215$ mm) occur in the near-surface layers of the principal trabeculae. They are more uniformly distributed over the thickness and decrease at increased length of the principal trabeculae ($l_1>0.215$ mm). It can be assumed that according to the von Mises is the maximum distortion energy theory, which claims that considered that failure in material occurs when the maximum von Mises stress equals the ultimate strength [41], cracks in the near-surface layers of the principal trabeculae first form in samples with short principal trabeculae, but not in samples with long principal trabeculae, where cracks can occupy the entire

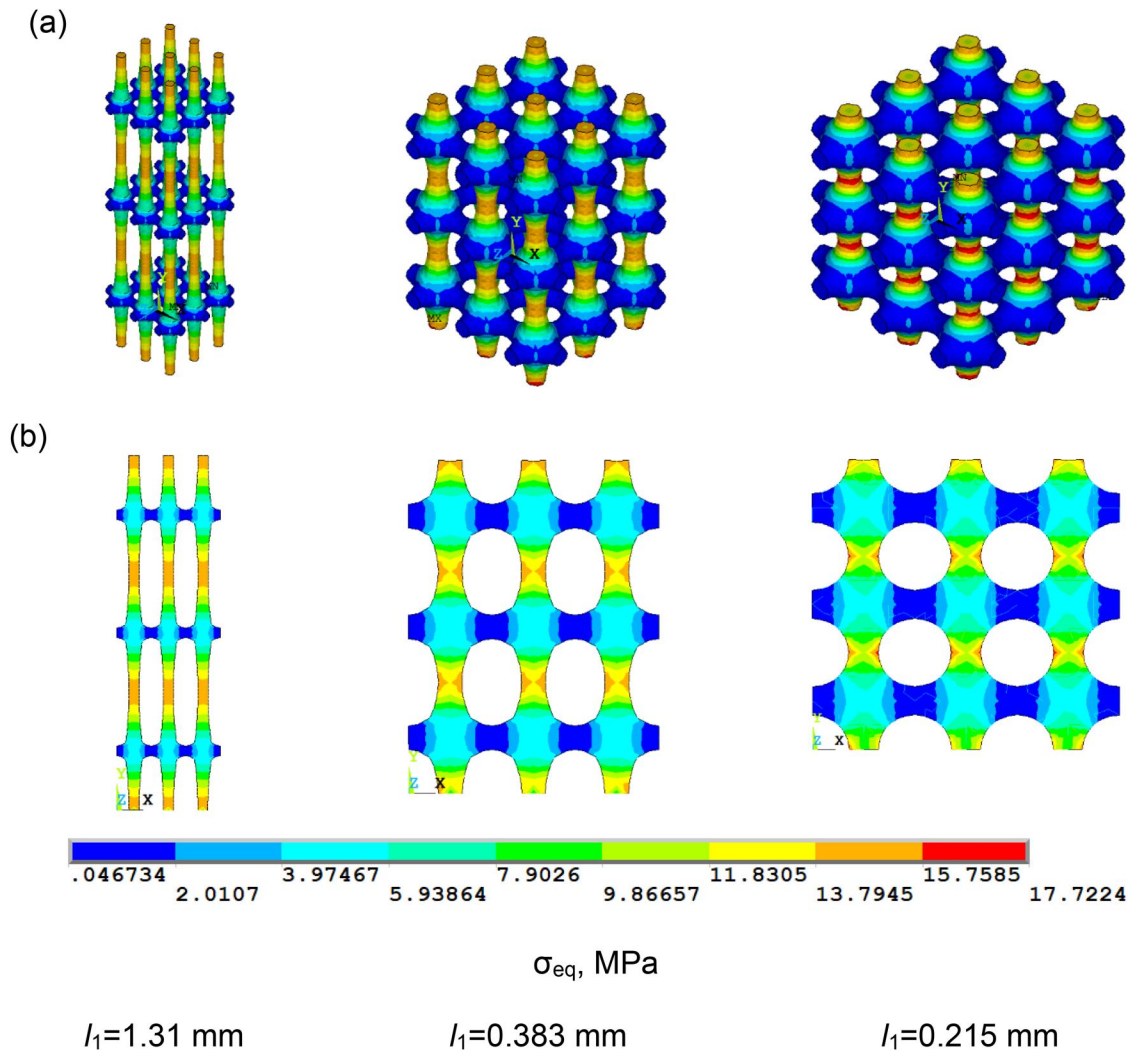


Figure 11. The von Mises stress distribution (a) over the surface and (b) inside model samples of cancellous bone tissue (section formed by the YX plane) with different lengths of the principal trabecula. Here, $l_2 = 0.215 \text{ mm}$, $t_1 = 0.162 \text{ mm}$, $t_2 = 0.162 \text{ mm}$, $\alpha = 0.1$.

thickness of the material of the principal trabeculae. The dependence of the maximum von Mises stresses on the principal trabeculae length in Figure 13 shows a decrease in values with an increase in the principal trabeculae length by 1.1 times.

3.4. The influence of the principal trabeculae length and the minerals mass fraction on the normal strain distribution in cancellous bone tissue fragments

Figures 14 and 15(a, b) show distribution of the normal axial strains ε_y , indicating that the maximum absolute compressive strains occur in the principal trabeculae. In samples with short principal trabeculae ($l_1=0.215 \text{ mm}$), the maximum absolute compressive axial strains occur in the near-surface layers of the principal trabeculae. They are uniformly distributed over the thickness in the middle part of the principal trabeculae and decrease at increased length of the principal trabecula ($l_1=1.31 \text{ mm}$). The maximum tensile strains occur in the secondary trabeculae in Figures 16(a, b) and 17(a, b).

Distribution of the normal strains ε_x , ε_z in Figures 14(c, d), 15(c, d), 16(c, d), and 17(c, d) indicates that the maximum tensile strains in samples with short principal trabeculae ($l_1=0.215 \text{ mm}$) occur in the near-surface layers of the central part of the principal trabeculae. They are more uniformly distributed over the thickness in the central part of the principal trabeculae at increased length of the principal trabecula ($l_1=1.31 \text{ mm}$). Comparison of the values of the normal strains ε_x , ε_y , and ε_z revealed that ε_z and ε_x are the maximum tensile normal strains, and ε_y strains are the maximum absolute compressive strains.

According to the theory of maximum normal strains, the destruction in material occurs when the maximum normal deformation reaches a limiting value [41]. Therefore, it can be assumed that cracks in the near-surface layers of the principal trabeculae form first in samples with short principal trabeculae, but not in samples with long principal trabeculae, where cracks can occupy the entire thickness of the material of the principal trabecula.

A change in the mass fraction of bone tissue minerals affects the value of the maximum and minimum normal strains. A fourfold change in the mass fraction of minerals

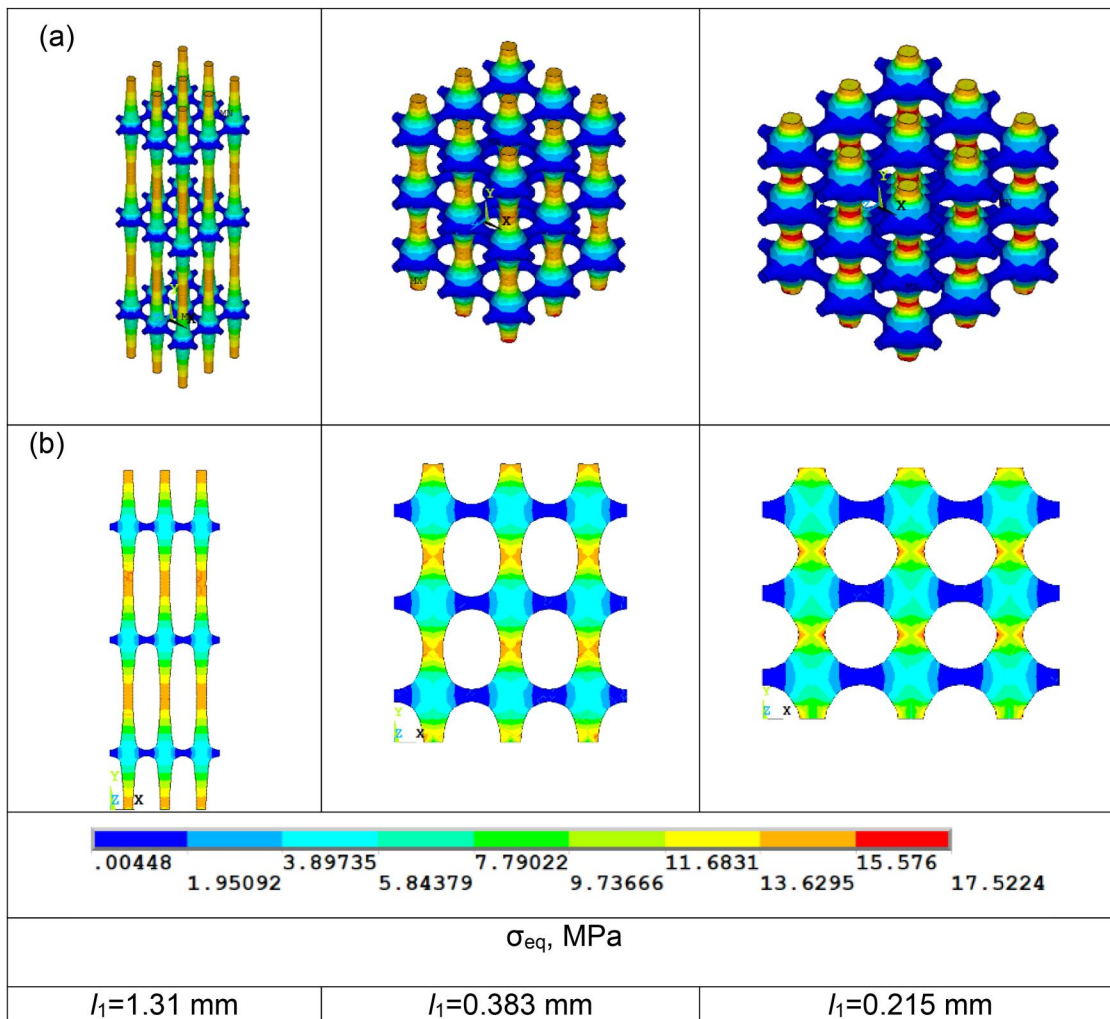


Figure 12. The von Mises stress distribution (a) over the surface and (b) inside model samples of cancellous bone tissue (section formed by the YX plane) with different lengths of the principal trabecula. Here, $l_2 = 0.215 \text{ mm}$, $t_1 = 0.162 \text{ mm}$, $t_2 = 0.109 \text{ mm}$, $\alpha = 0.4$.

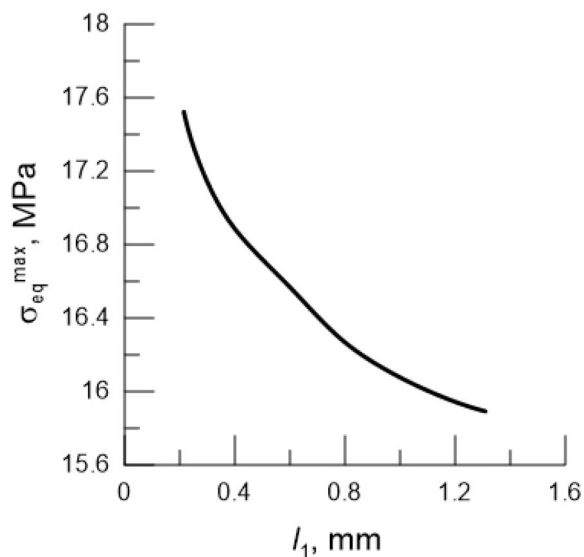


Figure 13. Dependence of the maximum von Mises stress of model cancellous bone tissue samples on the principal trabeculae length.

from 0.1 to 0.4 leads to a decrease in the values of the maximum tensile strains and maximum absolute values of the compressive ε_x and ε_y strains by a factor of 4.8.

3.5. The influence of the principal trabeculae length and minerals mass fraction on the value of the elastic longitudinal modulus and mU_x , mU_y , and mU_z parameters

Figure 18 presents the graphs for the effective longitudinal elastic modulus of a cancellous bone tissue sample with different mineral content and different thickness of the secondary trabeculae versus the length of the principal trabecula.

The effect of the secondary trabeculae thickness on the longitudinal elastic modulus is negligible. At increased mass fraction of minerals in bone tissue α , the longitudinal elastic modulus increases. The mass fraction of minerals increase from 0.1 to 0.4 (by a factor of 4) causes a 4.8-fold increase in the longitudinal elastic modulus of cancellous bone tissue

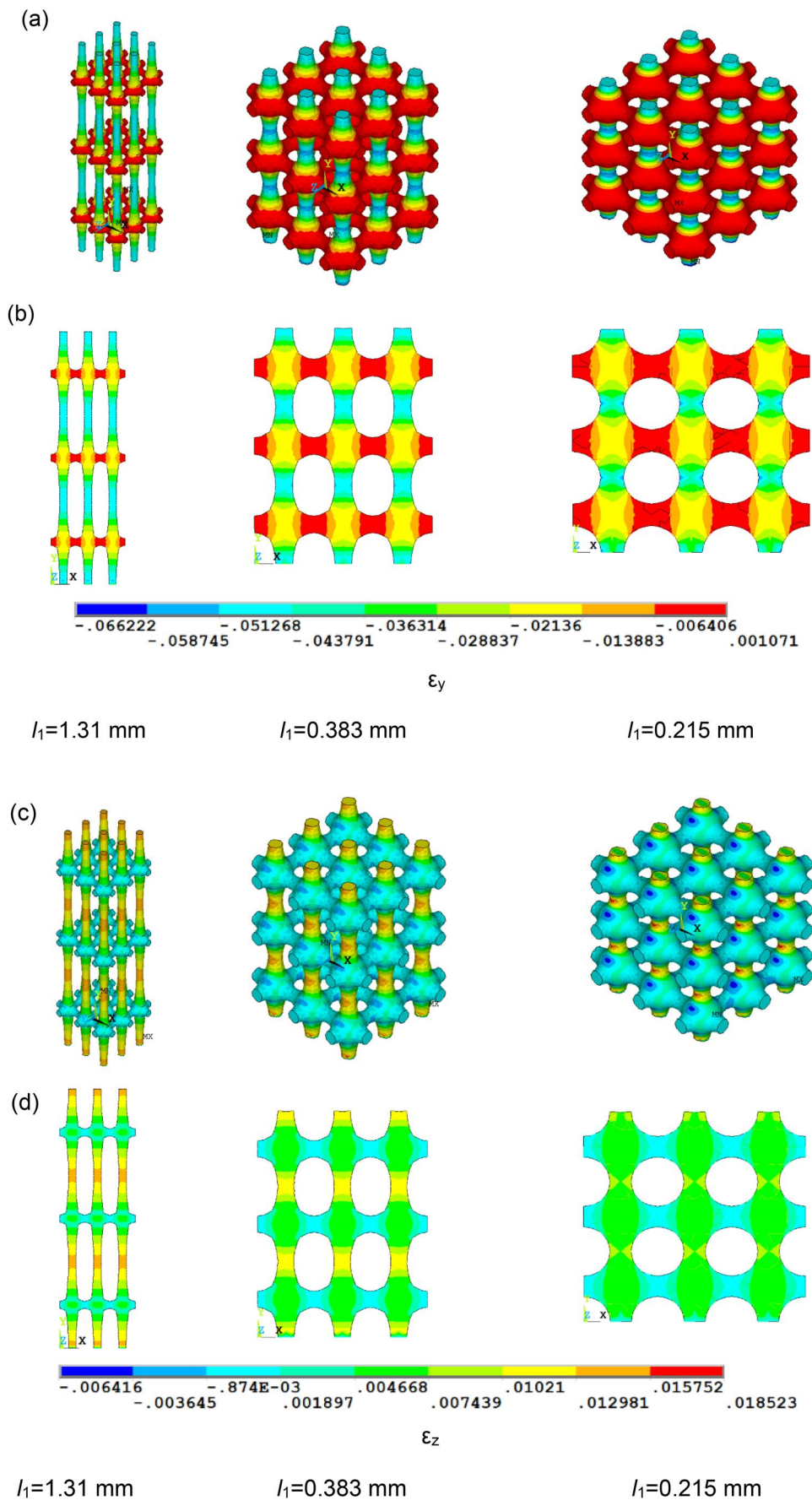


Figure 14. Distribution of normal strains (a, c) over the surface and (b, d) inside model samples of cancellous bone tissue (section formed by the YX plane) with different lengths of the principal trabecula. Here, $l_2 = 0.215$ mm, $t_1 = 0.162$ mm, $t_2 = 0.162$ mm, $\alpha = 0.1$.

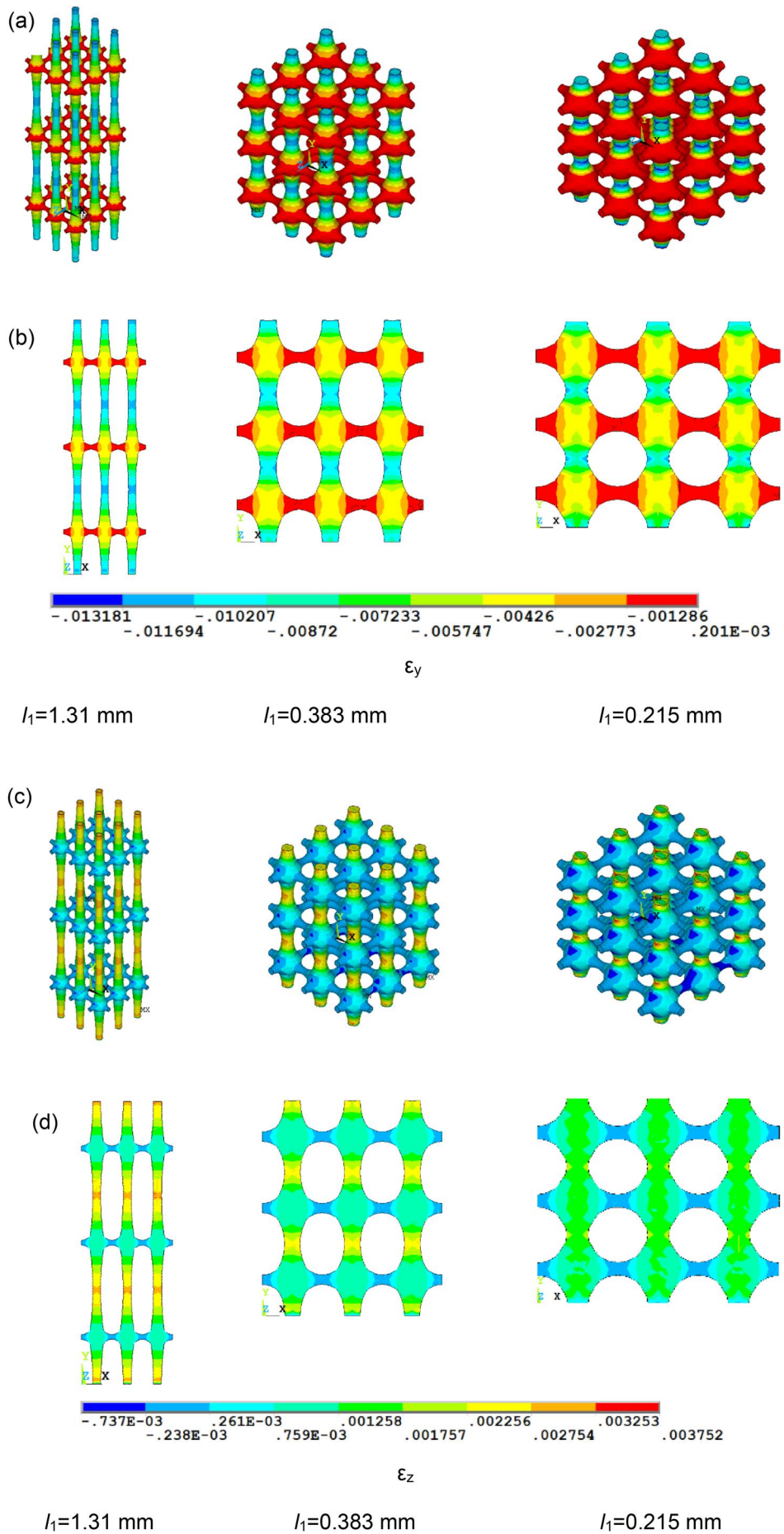


Figure 15. Distribution of normal strains (a, c) over the surface and (b, d) inside model samples of cancellous bone tissue (section formed by the YX plane) with different lengths of the principal trabecula. Here, $l_2 = 0.215 \text{ mm}$, $t_1 = 0.162 \text{ mm}$, $t_2 = 0.109 \text{ mm}$, $\alpha = 0.4$.

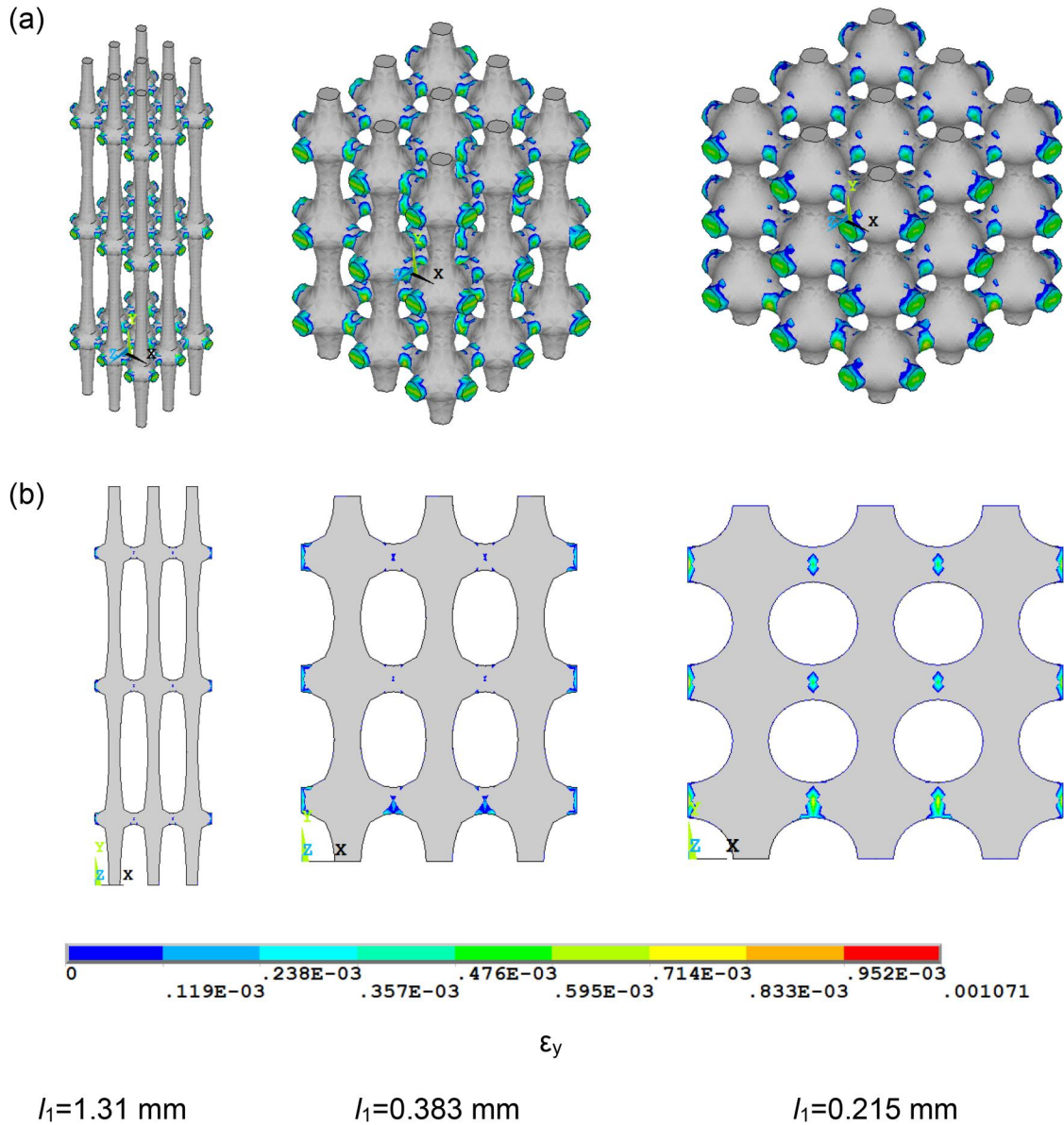


Figure 16. Distribution of tensile normal strains (a, c) over the surface and (b, d) inside model samples of cancellous bone tissue (section formed by the YX plane) with different lengths of the principal trabecula. Here, $l_2 = 0.215 \text{ mm}$, $t_1 = 0.162 \text{ mm}$, $t_2 = 0.162 \text{ mm}$, $\alpha = 0.1$.

samples, regardless of the length of the principal trabecula. The effective longitudinal elastic modulus of the bone sample decreases with increased length of the principal trabeculae of cancellous bone tissue. The increase in length of the principal trabeculae of cancellous bone tissue from 0.215 to 1.31 mm (by a factor of 6) triggers a 1.2-fold decrease in the elastic modulus, regardless of the mass fraction of minerals in the bone sample.

Approximation of curves in the Grapher program showed the power-law dependence of the longitudinal elastic modulus of cancellous bone tissue samples (in MPa) on the length of the principal trabecula (in mm):

$$E = A * l_1^{-B}, R^2 = 0.999 \quad (2)$$

Construction of dependencies of the A and B coefficients approximating expressions for the mass fraction of minerals

showed that B is constant, $B=0.114$, while A varies depending on the mass fraction as:

$$A = C * \alpha^D, R^2 = 0.999, \text{ where } C = 6286, \text{ and } D = 1.14 \quad (3)$$

The values of the coefficients B, C, and D may vary with the change in the principal trabecula thickness t_1 and the secondary trabecula length l_2 , which requires additional research.

The elastic modulus of the cancellous bone tissue model sample, which was similar to the laboratory one in Figure 2, was determined with respect to the volume fraction of the bone fragments with different lengths of the principal trabeculae and the mass fraction of minerals in the structure of the laboratory sample with $\alpha=0.1$. The calculated value was

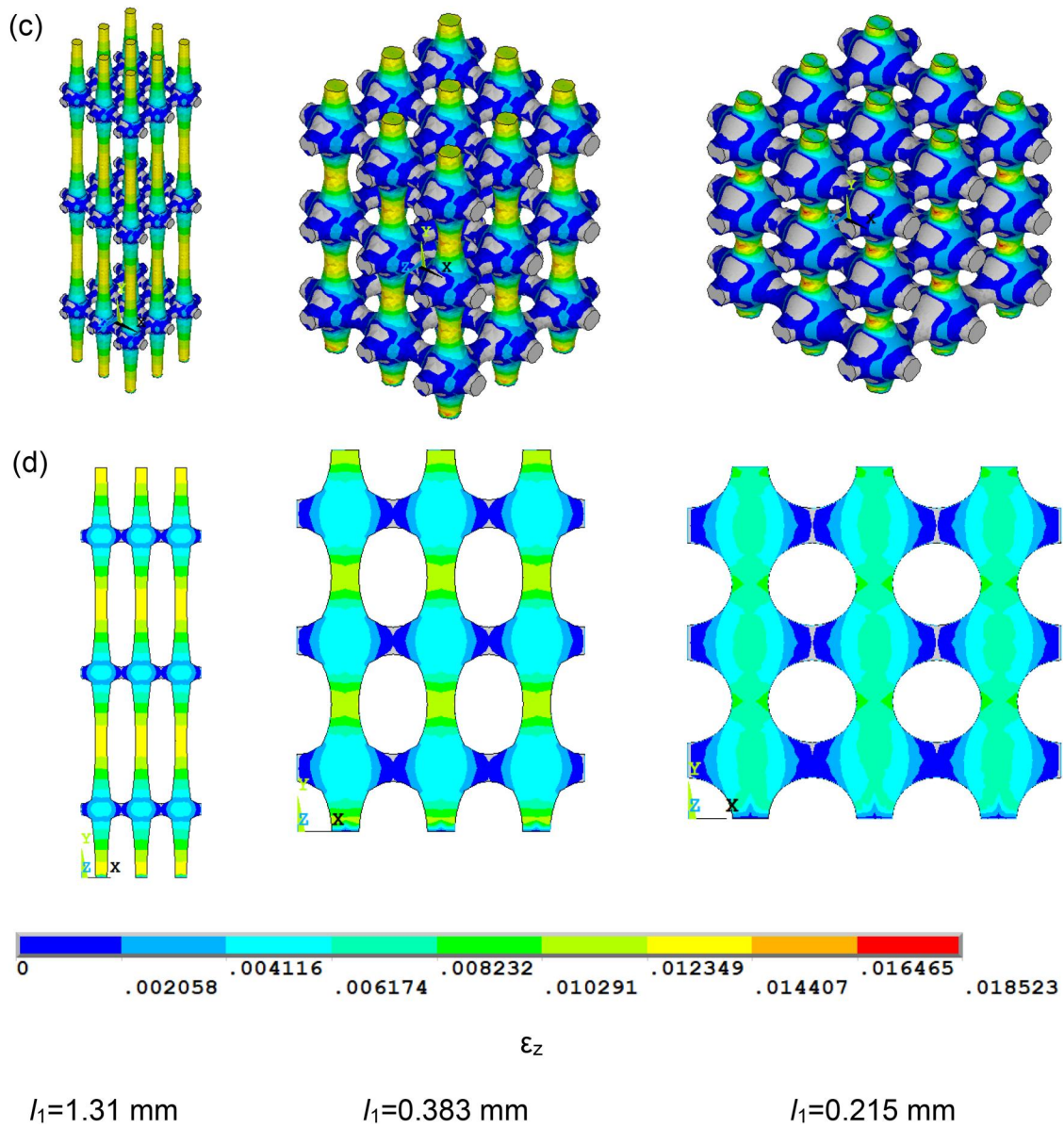


Figure 16. Continued.

equal to 482.12 MPa. Figure 19 compares stress–strain curves of the natural cancellous bone tissue sample and the model sample under uniaxial compression.

Parameters mU_y , mU_x , and mU_z for samples of cancellous bone tissue with varying thickness of secondary trabeculae are plotted in Figure 20 against the length of the primary trabecula. These graphs demonstrate that the influence of changing the thickness of secondary trabeculae on the mU_y , mU_x , mU_z parameters is insignificant. Increasing the mineral mass fraction in bone tissue, denoted as α , does not affect the considered parameters and, therefore, the nature of stress and strain distribution in the examined samples of cancellous bone tissue.

Increasing the length of the primary trabeculae of cancellous bone tissue from 0.215 to 1.31 mm (by a factor of 6) results in a 3.5-fold decrease in the values of mU_x and mU_z parameters, and a 1.07-fold increase in the mU_y parameter.

The approximation of the obtained dependencies allowed deriving the following expressions:

$$mU_y = F * l_1^G, R^2 = 0.999, \text{ where } F = 0.965, G = 0.0387 \quad (4)$$

$$mU_z = K * \ln(l_1) + M, R^2 = 0.999, \text{ where } K = -0.0183, M = 0.0174 \quad (5)$$

The values of the F , G , K , and M coefficients may vary with the change in the principal trabecula thickness t_1 and the secondary trabecula length l_2 , which requires additional research.

4. Discussion

This study investigated the stress–strain state of model fragments of cancellous bone tissue with different structure and

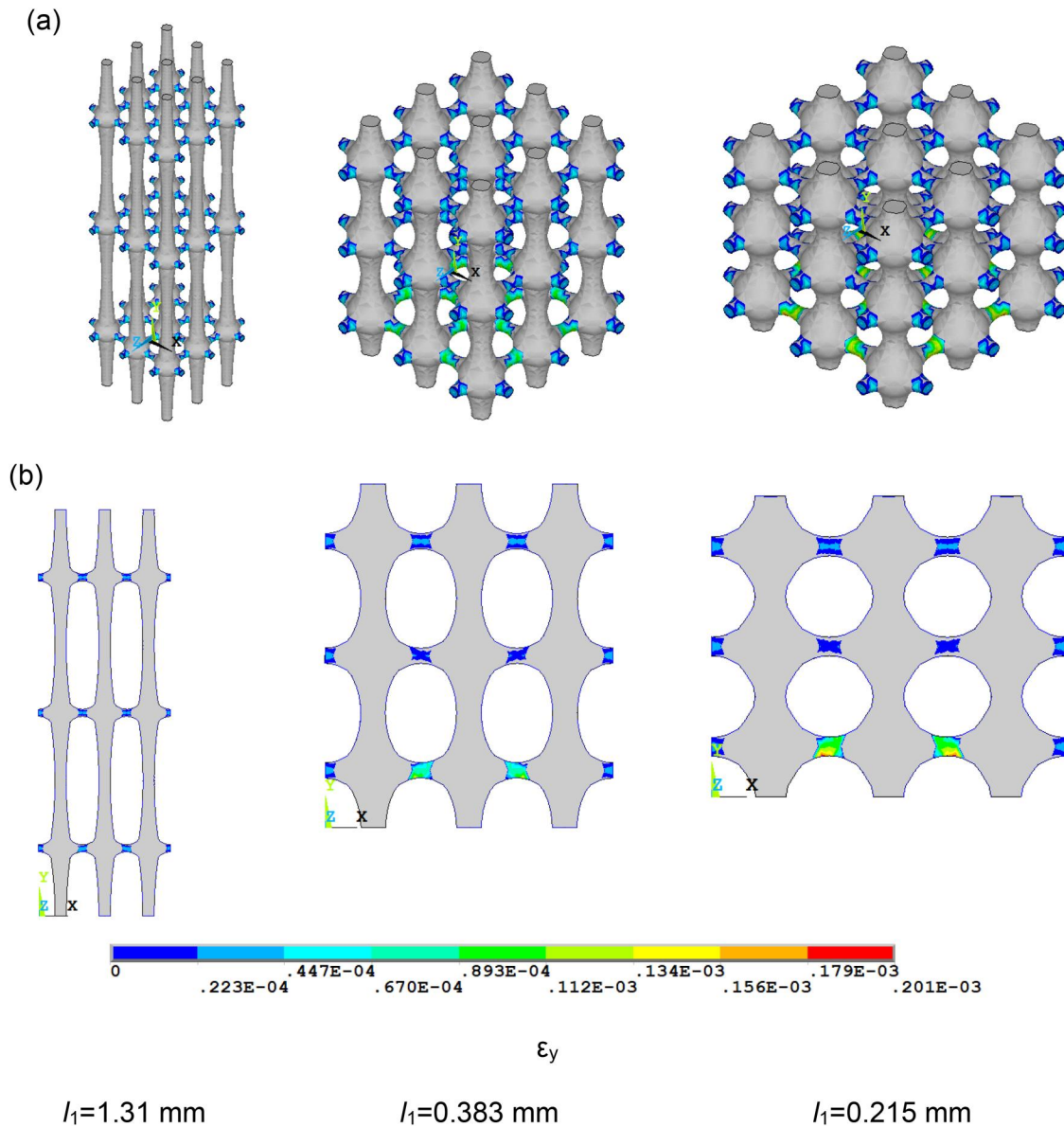


Figure 17. Distribution of tensile normal strains (a, c) over the surface and (b, d) inside model samples of cancellous bone tissue (section formed by the YX plane) with different lengths of the principal trabecula. Here, $l_2 = 0.215$ mm, $t_1 = 0.162$ mm, $t_2 = 0.109$ mm, $\alpha = 0.4$.

composition under uniaxial compression, and answered two questions. (1) What effective mechanical parameters reflect the nature and magnitude of realized stresses and strains? Parameters mU_y , mU_x , and mU_z were introduced to assess the degree of deformation responses of bone samples in three mutually perpendicular directions under uniaxial compression, reflecting the nature of stress and strain distribution in the bone tissue sample. The effective mechanical parameter reflecting the magnitude of realized stresses and strains is the effective longitudinal modulus of elasticity. It is proposed to use the considered effective characteristics (mU_x , mU_y , mU_z , and the longitudinal modulus of elasticity) in the selection and development of individual mechanically compatible osteoimplants, or components of joint prostheses or dental prostheses implanted directly into cancellous bone tissue. The assumption is that if these parameters are selected for a fixed type of loading, such as uniaxial

compression, in accordance with the parameters of the replaced fragment of bone tissue with a defined structure and composition, then the installation of such an implant in the body will help avoid bone tissue resorption at the bone-implant interface, or to minimize resorption, since implant micromovements relative to the bone also affect implantation outcome. It is also believed that the proposed parameters can be used to stimulate bone tissue growth after fractures or when it is necessary for bone tissue to grow through a porous implant. This can be achieved by deviating the proposed parameters in the desired direction, which requires additional research. The obtained values of the longitudinal elastic modulus of the model fragments of cancellous bone tissue do not contradict the experimental literature data [12–14, 42]. (2) The second question addressed in this study was how does the nature of stress and strain distribution, as well as their magnitudes, change

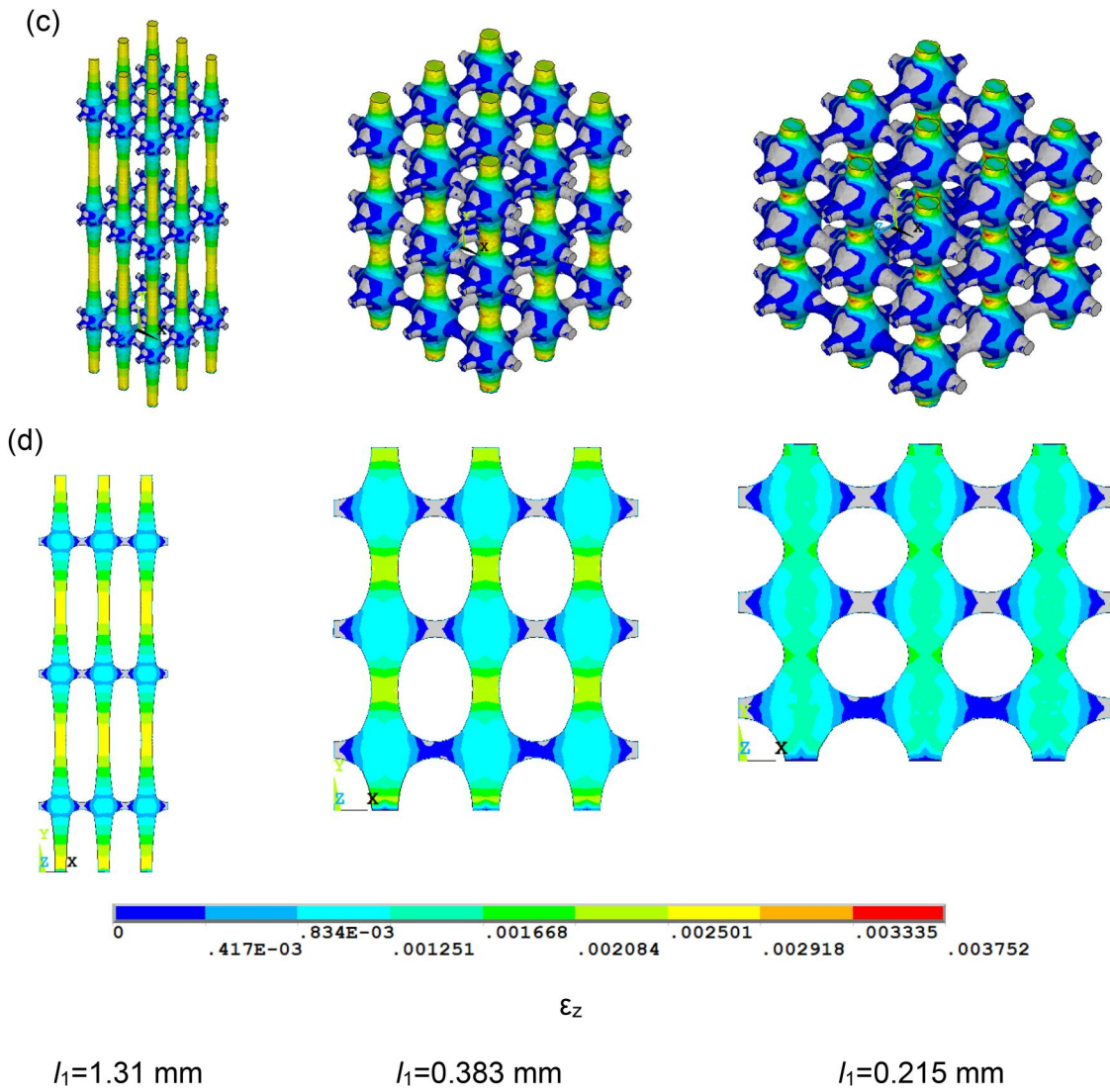


Figure 17. Continued.

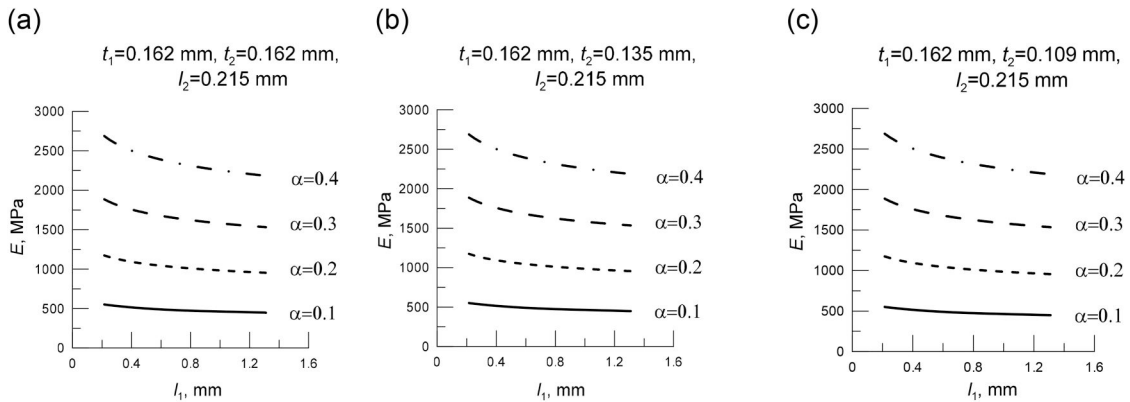


Figure 18. The effective longitudinal elastic modulus of a cancellous bone tissue samples with different mineral content and different thickness of the secondary trabeculae: (a) $t_2 = 0.162 \text{ mm}$, (b) $t_2 = 0.135 \text{ mm}$, (c) $t_2 = 0.109 \text{ mm}$ versus the length of the principal trabecula.

with variations in the structure and composition of cancellous bone tissue fragments, specifically with changes in the length of the primary trabecula, thickness of the secondary trabecula, and mineral mass fraction.

Analysis of the normal stresses and strains distribution in model samples of cancellous bone tissue with different lengths of the principal trabeculae under uniaxial compression along the Y axis revealed that the maximum absolute

compressive stresses σ_y and strains ε_y occur in the principal trabeculae. It has been demonstrated that the thickness of secondary trabeculae does not affect the nature and magnitude of stress and strain distribution in cancellous bone tissue. Changes in the mineral mass fraction only influence the magnitude of realized stresses and strains and do not impact the nature of their distribution.

A similar conclusion suggests that trabeculae aligned along the main trabecular axis bear the majority of the mechanical loads, while trabeculae distributed laterally contribute less to stiffness and strength, primarily facilitating the transmission and distribution of stresses between the

trabeculae [43]. Another study numerically demonstrated that the longitudinal trabecular plate is the main carrier of compressive stresses [44].

Analysis of the pattern of the von Mises stress distribution and normal strains showed that cracks in the near-surface layers of the principal trabeculae form first in samples with short principal trabeculae, but not in samples with long principal trabeculae, where cracks can occupy the entire thickness of the material of the principal trabecula.

It was demonstrated numerically in Ref. [45] that cracks can form in cancellous bone tissue, both on the surface and inside trabeculae, associated with uneven mineralization. In our case, we associate this with changes in the length of the primary trabeculae. All results of this work are valid for the case of linear elastic mechanical behavior.

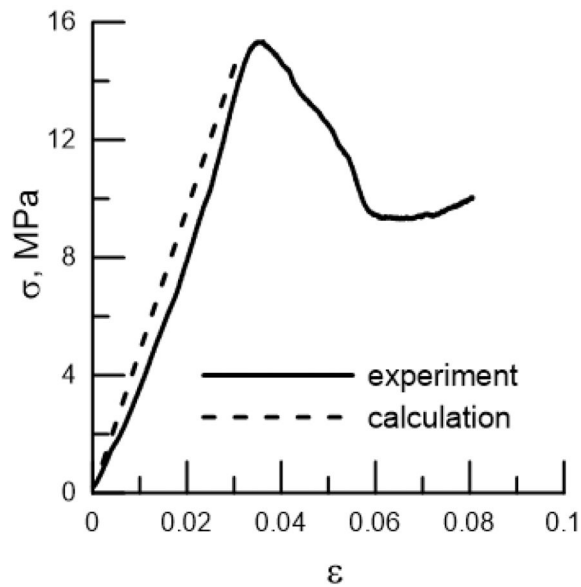


Figure 19. Stress–strain curves of the natural cancellous bone tissue sample and the model sample under uniaxial compression.

5. Conclusions

The study of the stress–strain state of model fragments of cancellous bone tissue with different composition and structure under uniaxial compression has been conducted. Parameters mU_x , mU_y , mU_z have been proposed, determining the nature of stress and strain distribution in bone tissue. Along with the longitudinal modulus of elasticity reflecting the magnitudes of realized stresses and strains, it is suggested to use these parameters for the development and selection of individual mechanically compatible osteoimplants, components for joint prostheses or dental prostheses, which are placed directly into spongy bone tissue. The obtained parameters are calculated using the linear elastic stress–strain state, and are relative; therefore, the magnitude of the compressive load will in no way affect the conclusions obtained in this work.

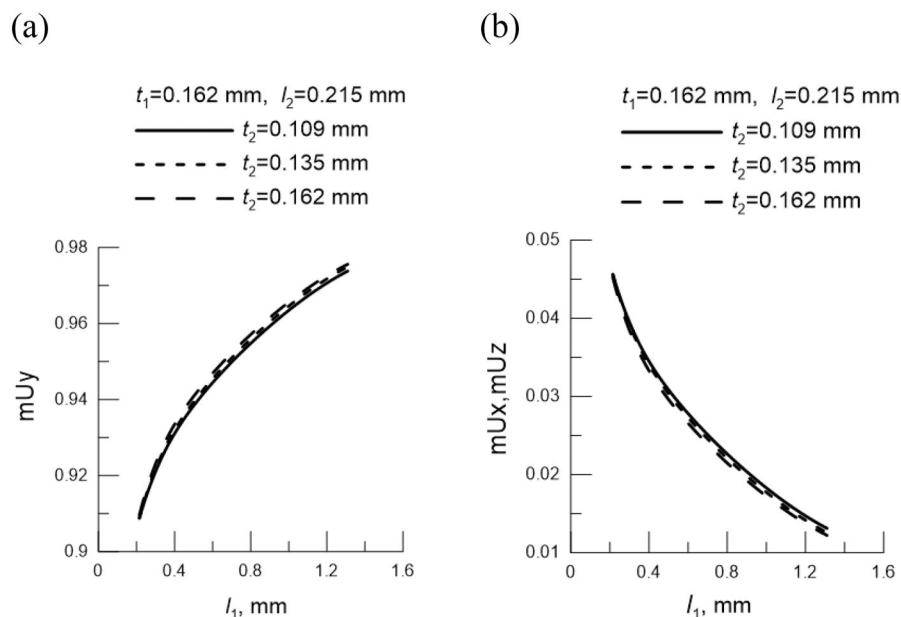


Figure 20. Dependence of the parameters (a) mU_y , (b) mU_x and mU_z for samples of cancellous bone tissue with varying thickness of secondary trabeculae on the length of the primary trabecula.

Acknowledgments

This research was supported by the Ministry of Science and Higher Education of the Russian Federation project No. FSWM-2020-0022.

Author contribution statement

Tatyana Chaykovskaya: Conceptualization, investigation; writing—original draft preparation, writing—review and editing. Ekaterina Marchenko: Methodology, project administration, funding acquisition. Yuri Yasenjuk: Methodology, writing—original draft preparation. Gulsharat Baigonakova: Visualization, investigation; writing—review and editing. Alex Volinsky: Visualization, investigation; writing—review and editing.

Disclosure statement

No potential conflict of interest was reported by the author(s).

ORCID

Tatyana V. Chaykovskaya  <http://orcid.org/0000-0003-1938-3083>

References

- [1] J. Wolff, *The Law of Bone Remodelling*. Berlin, Germany: Springer, 1986.
- [2] A. S. Avrunin and E. A. Tses, “The birth of a new scientific field – Biomechanics of the skeleton. Julius Wolff and his work ‘Das Gesetz der Transformation der Knochen’,” *Hist. Med.*, vol. 3, no. 4, pp. 447–461, 2016. DOI: [10.17720/2409-5583.t3.4.2016.36q](https://doi.org/10.17720/2409-5583.t3.4.2016.36q).
- [3] R. B. Martin, D. B. Burr, and N. A. Sharkey, 1998. *Skeletal Tissue Mechanics*, 2nd ed. New York: Springer-Verlag.
- [4] I. Knets, “General principles of bone tissue testing,” *Acta Bioeng. Biomech.*, vol. 1, pp. 55–56, 1999.
- [5] I. Sevostianov and M. Kachanov, “Impact of the porous microstructure on the overall elastic properties of the osteonal cortical bone,” *J. Biomech.*, vol. 33, no. 7, pp. 81–888, 2000. DOI: [10.1016/s0021-9290\(00\)00031-2](https://doi.org/10.1016/s0021-9290(00)00031-2).
- [6] T. M. Keaveny, E. F. Morgan, and O. C. Yeh, Chapter 8 Bone Mechanics in Standard Handbook of Biomedical Engineering and Design, M. Kutz, Ed. New York: McGraw-Hill, pp. 8.1–8.23, 2003.
- [7] T. M. Keaveny, E. F. Morgan, G. L. Niebur, and O. C. Yeh, “Biomechanics of trabecular bone,” *Annu. Rev. Biomed. Eng.*, vol. 3, no. 1, pp. 307–333, 2001. DOI: [10.1146/annurev.bioeng.3.1.307](https://doi.org/10.1146/annurev.bioeng.3.1.307).
- [8] S. C. Cowin, “Wolff’s law of trabecular architecture at remodeling equilibrium,” *J. Biomech. Eng.*, vol. 108, no. 1, pp. 83–88, 1986. DOI: [10.1115/1.3138584](https://doi.org/10.1115/1.3138584).
- [9] S. C. Cowin, *Bone Mechanics Handbook*, 2nd ed. New York: CRC Press, 2001, 1136 p.
- [10] S. J. Mellon and K. E. Tanner, “Bone and its adaptation to mechanical loading: A review,” *Int. Mater. Rev.*, vol. 57, no. 5, pp. 235–255, 2012. DOI: [10.1179/1743280412Y.0000000008](https://doi.org/10.1179/1743280412Y.0000000008).
- [11] M. Racila and J. M. Crolet, “Nano and macro structure of cortical bone: Numerical investigations,” *Mech. Adv. Mater. Struct.*, vol. 14, no. 8, pp. 655–663, 2007. DOI: [10.1080/15376490701673193](https://doi.org/10.1080/15376490701673193).
- [12] N. Rosa, M.F.S.F. Moura, S. Olhero, R. Simoes, F.D. Magalhães, A.T. Marques, J.P.S. Ferreira, A.R. Reis, M. Carvalho, and M. Parente, “Bone: An outstanding composite material,” *Appl. Sci.*, vol. 12, no. 7, pp. 3381, 2022. DOI: [10.3390/app12073381](https://doi.org/10.3390/app12073381).
- [13] H. Orava, L. Huang, S.P. Ojanen, J.T.A. Mäkelä, M.A.J. Finnilä, S. Saarakkala, W. Herzog, R.K. Korhonen, J. Töyräs, and P. Tanska, “Changes in subchondral bone structure and mechanical properties do not substantially affect cartilage mechanical responses – A finite element study,” *J. Mech. Behav. Biomed. Mater.*, vol. 128, pp. 105129, 2022. DOI: [10.1016/j.jmbbm.2022.105129](https://doi.org/10.1016/j.jmbbm.2022.105129).
- [14] F. Hamandi and T. Goswami, “Hierarchical structure and properties of the bone at nano level,” *Bioengineering*, vol. 9, no. 11, pp. 677, 2022. DOI: [10.3390/bioengineering9110677](https://doi.org/10.3390/bioengineering9110677).
- [15] F. Hamandi and T. Goswami, “Macrodamage accumulation model for a human femur,” *Appl. Bionics Biomech.*, vol. 2017, pp. 4539178, 2017. DOI: [10.1155/2017/4539178](https://doi.org/10.1155/2017/4539178).
- [16] E. Novitskaya, E. Hamed, J. Li, Z. Manilay, I. Jasiuk, and J. McKittrick, “Hierarchical structure of porosity in cortical and trabecular bones,” *Mater. Res. Soc. Symp. Proc.*, vol. 1420, pp. 24–20, 2012. DOI: [10.1557/opl.2012.488](https://doi.org/10.1557/opl.2012.488).
- [17] S. Asadollahi and M. Dehestani, “Effective elastic constants of cortical bone at lamellae and osteon levels considering mineral composition and lamellar arrangement,” *Mech. Adv. Mater. Struct.*, vol. 29, no. 25, pp. 3961–3981, 2022. DOI: [10.1080/15376494.2021.1916135](https://doi.org/10.1080/15376494.2021.1916135).
- [18] E. Novitskaya, P.-Y. Chen, E. Hamed, L. Jun, V.A. Lubarda, I. Jasiuk, and J. McKittrick, “Recent advances on the measurement and calculation of the elastic moduli of cortical and trabecular bone: A review,” *Theor. Appl. Mech. (Belgr.)*, vol. 38, no. 3, pp. 209–297, 2011. DOI: [10.2298/TAM1103209N](https://doi.org/10.2298/TAM1103209N).
- [19] S. Nobakhti, “Nano-scale modeling of energy dissipation in a single lamella reveals the significant contribution of collagen-mineral sliding to intrinsic bone toughness,” *Mech. Adv. Mater. Struct.*, pp. 1–20, 2024. DOI: [10.1080/15376494.2024.2395506](https://doi.org/10.1080/15376494.2024.2395506).
- [20] E. A. A. Alkebsi, T. Outtas, A. Almutawakel, H. Ameddah, and T. Kanit, “Design of mechanically compatible lattice structures cancellous bone fabricated by fused filament fabrication of Z-ABS material,” *Mech. Adv. Mater. Struct.*, vol. 30, no. 11, pp. 2269–2283, 2023. DOI: [10.1080/15376494.2022.2053904](https://doi.org/10.1080/15376494.2022.2053904).
- [21] A. Sorrentino and D. Castagnetti, “Negative Poisson’s ratio lattice for designing vertebral biomaterials,” *Mech. Adv. Mater. Struct.*, vol. 29, no. 27, pp. 6626–6633, 2022. DOI: [10.1080/15376494.2021.1983089](https://doi.org/10.1080/15376494.2021.1983089).
- [22] T. Lee, R. R. Garlapati, K. Lam, P.V.S. Lee, Y.-S. Chung, J.B. Choi, T.B.C. Vincent, and S.D. De, “Fast tool evaluation of iliac crest tissue elastic properties using the reduced-basis methods,” *J. Biomech. Eng.*, vol. 132, no. 12, pp. 121009, 2010. DOI: [10.1115/1.4001254](https://doi.org/10.1115/1.4001254).
- [23] D. Ulrich, B. van Rietbergen, H. Weinans, and P. Rügsegger, “Finite element analysis of trabecular bone structure: A comparison of image-based meshing techniques,” *J. Biomech.*, vol. 31, no. 12, pp. 1187–1192, 1998. DOI: [10.1016/s0021-9290\(98\)00118-3](https://doi.org/10.1016/s0021-9290(98)00118-3).
- [24] T. Adachi, K. Tsubota, Y. Tomita, and S. J. Hollister, “Trabecular surface remodelling simulation for cancellous bone using microstructural voxel finite element models,” *J. Biomech. Eng.*, vol. 123, no. 5, pp. 403–409, 2001. DOI: [10.1115/1.1392315](https://doi.org/10.1115/1.1392315).
- [25] J. T. Koontz, G. T. Charas, and R. E. Guldberg, “A microstructural finite element simulation of mechanically induced bone formation,” *J. Biomech. Eng.*, vol. 123, no. 6, pp. 607–612, 2001. DOI: [10.1115/1.1406951](https://doi.org/10.1115/1.1406951).
- [26] R. Pivec, A. J. Johnson, S. C. Mears, and M. A. Mont, “Hip arthroplasty,” *Lancet*, vol. 380, no. 9855, pp. 1768–1777, 2012. DOI: [10.1016/S0140-6736\(12\)60607-2](https://doi.org/10.1016/S0140-6736(12)60607-2).
- [27] T. Karachalios, G. Komnos, and A. Koutalos, “Total hip arthroplasty: Survival and modes of failure,” *EFORT Open Rev.*, vol. 3, no. 5, pp. 232–239, 2018. DOI: [10.1302/2058-5241.3.170068](https://doi.org/10.1302/2058-5241.3.170068).
- [28] S. Hosseini, R. Claramunt, M. Ibáñez, and A. Ros, “Diagnosis of femoral implant loosening after total hip replacement by analysis of natural frequency,” *Mech. Adv. Mater. Struct.*, vol. 31, no. 5, pp. 1125–1134, 2024. DOI: [10.1080/15376494.2022.2131946](https://doi.org/10.1080/15376494.2022.2131946).
- [29] A. Ouldayerou, L. Aminallah, A. Merdji, A. Mehboob, and H. Mehboob, “Finite element analyses of porous dental implant designs based on 3D printing concept to evaluate biomechanical

- behaviors of healthy and osteoporotic bones,” *Mech. Adv. Mater. Struct.*, vol. 30, no. 11, pp. 2328–2340, 2023. DOI: [10.1080/15376494.2022.2053908](https://doi.org/10.1080/15376494.2022.2053908).
- [30] H. Mehboob, A. Mehboob, F. Abbassi, F. Ahmad, A.S. Khan, and S. Miran, “Bioinspired porous dental implants using the concept of 3D printing to investigate the effect of implant type and porosity on patient’s bone condition,” *Mech. Adv. Mater. Struct.*, vol. 29, no. 27, pp. 6011–6025, 2022. DOI: [10.1080/15376494.2021.1971347](https://doi.org/10.1080/15376494.2021.1971347).
- [31] P. Liu, J. Tu, W. Wang, Z. Li, Y. Li, X. Yu, Z. Zhang, “Effects of mechanical stress stimulation on function and expression mechanism of osteoblasts,” *Front. Bioeng. Biotechnol.*, vol. 10, pp. 830722, 2022. DOI: [10.3389/fbioe.2022.830722](https://doi.org/10.3389/fbioe.2022.830722).
- [32] M. Edamoto, Y. Kuroda, M. Yoda, K. Kawaai, and K. Matsuo, “Trans-pairing between osteoclasts and osteoblasts shapes the cranial base during development,” *Sci. Rep.*, vol. 9, no. 1, pp. 1956, 2019. DOI: [10.1038/s41598-018-38471-w](https://doi.org/10.1038/s41598-018-38471-w).
- [33] H. Matsuno, B. Li, H. Okawara, Y. Toyoshima, C. Xie, M. Khan, N. Murakami, K. Aoki, and N. Wakabayashi, “Effect of tension and compression on dynamic alveolar histomorphometry,” *J. Mech. Behav. Biomed. Mater.*, vol. 138, pp. 105666, 2023. DOI: [10.1016/j.jmbbm.2023.105666](https://doi.org/10.1016/j.jmbbm.2023.105666).
- [34] T. Kolmakova, “Computer modeling of the structure of the cortical and trabecular bone tissue,” *AIP Conf. Proc.*, vol. 1683, 020087, 2015.
- [35] Y. N. Lastovkina and T. V. Kolmakova, “Computer modelling of the microstructure of the trabecular bone fragments for the study of stress-strain state,” *J. Phys. Conf. Ser.* vol. 769, 012020, 2016. DOI: [10.1088/1742-6596/769/1/012020](https://doi.org/10.1088/1742-6596/769/1/012020).
- [36] D. Dagan, M. Be’ery, and A. Gefen, “Single-trabecula building block for large-scale finite element models of cancellous bone,” *Med. Biol. Eng. Comput.*, vol. 42, no. 4, pp. 549–556, 2004. DOI: [10.1007/BF02350998](https://doi.org/10.1007/BF02350998).
- [37] R. M. Christensen, *Mechanics of Composite Materials*. New York: Wiley, 1979.
- [38] Ł. Cyganik, M. Binkowski, G. Kokot, T. Rusin, P. Popik, F. Bolechała, R. Nowak, Z. Wróbel, and A. John, “Prediction of Young’s modulus of trabeculae in microscale using macro-scale’s relationships between bone density and mechanical properties,” *J. Mech. Behav. Biomed. Mater.*, vol. 36, pp. 120–134, 2014. DOI: [10.1016/j.jmbbm.2014.04.011](https://doi.org/10.1016/j.jmbbm.2014.04.011).
- [39] T. V. Kolmakova, “Computer-aided study of the mechanical behavior of the jaw bone fragments under uniaxial compression,” *AIP Conf. Proc.*, vol. 1760, 020030, 2016. DOI: [10.1063/1.4960249](https://doi.org/10.1063/1.4960249).
- [40] T. V. Chaykovskaya, “Effective mechanical parameters of bone tissue samples for the selection of individual osteoimplants,” *Tomsk State Univ. J. Math. Mech.*, vol. 89, no. 89, pp. 162–175, 2024. DOI: [10.17223/19988621/89/12](https://doi.org/10.17223/19988621/89/12).
- [41] M. S. Kazimi, N. E. Todreas, and L. Wolf, Introduction to structural mechanics. MIT OpenCourseWare. 22.312 Engineering of nuclear reactors I.4, 61, 2001.
- [42] D. R. Carter, G. H. Schwab, and D. M. Spengler, “Tensile fracture of cancellous bone,” *Acta Orthop. Scand.*, vol. 51, no. 5, pp. 733–741, 1980. DOI: [10.3109/17453678008990868](https://doi.org/10.3109/17453678008990868).
- [43] B. Zhou, X.S. Liu, J. Wang, X.L. Lu, A.J. Fields, X.E. Guo, “Dependence of mechanical properties of trabecular bone on plate-rod microstructure determined by individual trabecula segmentation (ITS),” *J. Biomech.*, vol. 47, no. 3, pp. 702–708, 2014. DOI: [10.1016/j.jbiomech.2013.11.039](https://doi.org/10.1016/j.jbiomech.2013.11.039).
- [44] J. Wang, G. J. Kazakia, B. Zhou, X. T. Shi, and X. E. Guo, “Distinct tissue mineral density in plate- and rod-like trabeculae of human trabecular bone,” *J. Bone Miner. Res.*, vol. 30, no. 9, pp. 1641–1650, 2015. DOI: [10.1002/jbmr.2498](https://doi.org/10.1002/jbmr.2498).
- [45] A.M. Torres, J.B. Matheny, T.M. Keaveny, D. Taylor, C.M. Rinnac, and C.J. Hernandez, “Material heterogeneity in cancellous bone promotes deformation recovery after mechanical failure,” *Proc. Natl. Acad. Sci. U S A*, vol. 113, no. 11, pp. 2892–2897, 2016. DOI: [10.1073/pnas.1520539113](https://doi.org/10.1073/pnas.1520539113).